TECHNICAL ARTICLE

Lattice Defects Generated by Cyclic Thermomechanical Loading of Superelastic NiTi Wire

Ondřej Tyc[1,3] · Luděk Heller[1,2] · Petr Šittner[1,2]

Abstract Cyclic instability of stress–strain–temperature functional responses of NiTi is presumably due to the plastic deformation accompanying martensitic transformation proceeding under external stress. In order to obtain systematic experimental evidence on this, we have performed series of cyclic thermomechanical loading tests (10 cycles) on superelastic NiTi wires with nanocrystalline microstructure, evaluated accumulated unrecovered strains and analysed permanent lattice defects created during the cycling by TEM. The accumulated unrecovered strains and density of lattice defects increased with increasing temperature and stress, at which the forward and/or reverse transformation proceeded. It did not correlate with the temperature and stress applied in the test as such. If the martensitic transformation proceeded at low stress (<100 MPa), the cyclic stress–strain–temperature responses of the wire were found to be almost stable (only marginal accumulated unrecovered strain and few isolated dislocation loops and segments were generated during the thermomechanical cycling). This was the case in thermal cycling at low stresses or in cyclic shape memory test. If the forward and/or reverse martensitic transformation proceeded under large external stress (>250 MPa), the responses were very unstable (large accumulated unrecovered strains and high density of dislocations and deformation bands). A scheme allowing for estimating the cyclic instability of functional behaviours of various NiTi wires in wide range of thermomechanical loading tests was introduced.

Introduction

NiTi-based shape memory alloys display superelasticity and shape memory effects derived from cubic to monoclinic martensitic transformation [1]. Although the functional responses of NiTi derived from this transformation have already been utilized in engineering applications, many more exciting applications would become a reality, if cyclic instability of the stress–strain–temperature response of NiTi in cyclic thermomechanical loads could be improved or at least predicted. It has been known from early days of SMA research that shape memory and superelastic NiTi alloys are relatively prone to plastic deformation and must be strengthened to exhibit recoverable martensitic transformation without permanent deformation. The most common ways how the strengthening is achieved involve cold work/annealing [2] and Ti_3Ni_4 precipitation [3]. Nevertheless, even the strengthened NiTi alloys frequently display considerable cyclic instability in

✉ Petr Šittner
sittner@fzu.cz

1 Institute of Physics of the CAS, Na Slovance, 1992/2, 18221 Prague, Czechia

2 Nuclear Physics Institute of the CAS, Husinec - Řež 130, 250 68 Řež, Czechia

3 Faculty of Nuclear Sciences and Physical Engineering, CTU Prague, Prague 2, Czechia

thermomechanical loads posing serious problems for engineering applications.

In ideal case, martensitic transformation proceeding in a closed-loop thermomechanical cycle shall bring completely reversible strains and shall leave behind no permanent lattice defects (sample shape is restored no lattice defects remain in the austenitic microstructure on unloading and heating). The cyclic stress–strain–temperature thermomechanical response of ideal NiTi shall be stable in closed-loop thermomechanical load test up to ∼ 6% strain, just like in the case of true elastic deformation. In reality, this is almost never the case, since plastic deformation in some extent accompanies the cyclic martensitic transformation. If plastic deformation occurs during the closed-loop thermomechanical loading cycle, shape is not recovered completely, and permanent lattice defects remain in the microstructure and stress–strain–temperature response in subsequent cycle becomes different. The stress–strain–temperature response of NiTi element upon cycling gradually changes due to these plastic deformation processes generating permanent lattice defects and internal stresses in the austenitic microstructure. The activity of the plastic deformation processes accompanying martensitic transformation in thermomechanically cycled superelastic NiTi wires can thus be analysed by evaluating the cyclic instability of the stress–strain–temperature response [4], unrecovered strain [5, 6] and permanent lattice defects left in the microstructure of the cycled wire [6, 7].

While the cyclic instability of functional responses of NiTi (called functional fatigue [8]) represents a problem to be solved for many promising NiTi applications, limited number of cycles till failure (structural fatigue [9] due to nucleation and propagation of fatigue cracks) is a key barrier for further growth of NiTi superelastic technologies. It may but need not be related to the plastic deformation accompanying phase transformation. However, since crack nucleation and propagation is governed by the activity of dislocation slip processes accompanying the martensitic transformation, it is very likely that functional fatigue and structural fatigue are somehow related, though it still remains to be found how [10].

We have recently performed systematic experiments [5] designed to evaluate the unrecovered strains in thermomechanically loaded superelastic NiTi wires possessing nanograin microstructure. In contrast to the residual strains, unrecovered strains cannot be recovered by heating far above the A_f temperature. Based on the obtained results, we have proposed that unrecovered strains are generated in thermomechanically loaded NiTi, only when martensitic transformation proceeds under elevated external stress and that the amount of unrecovered strain increases with increasing stress at which the transformation proceeds. Since the forward and reverse martensitic transformations proceed in mechanical (thermal) cycles at different stresses (temperatures), the generation of unrecovered strains by the forward and reverse MT was treated separately in [5]. However, since we were not able to observe the lattice defects created by the martensitic transformation, in the nanograined microstructure of the alloy, evaluating the involvement of the individual deformation processes in accumulation of unrecovered strain was not possible.

Concerning the lattice defects created upon thermomechanical cycling through transformation range, there is rather limited statistically relevant experimental evidence on the slip dislocations created by cycling [11–17], but there is variety of opinions on their origin in the literature [5, 16, 18–20]. The observed lattice defects include dislocation loops [11], slip dislocations in glide planes [12, 13], slip dislocations at habit plane interfaces [14, 15, 19], and deformation bands with {114} austenite twins and/or residual B19′ martensite [7, 17, 21–23]. Simplest explanation of the observed slip dislocations in austenite would be based on the consideration of slip or twinning in the austenite proceeding in parallel with the martensitic transformation [16, 24, 25].Theoretical analysis of various possible slip systems in B2 austenite reported in the literature [16] favours the activity of {110}/ < 001 > slip system, which was most frequently observed in experiments [13]. There is only one slip system (001)/[100] in the monoclinic B19′ martensite, the activity of which is considered in the literature [18]. As regards the deformation bands, it has been known since late 80ties that deformation bands containing family of austenite twins from the [1–10] zone {112}, {113}, {225}, {114} [26–34] appear in the microstructure of heavily deformed NiTi. Nishida et al. [29] who analysed deformation bands observed in NiTiFe strip deformed in tension at 200 °C up to ∼ 20% strain found that they contain mainly {114} austenite twins. Deformation bands containing {114} austenite twins were, however, later observed also in NiTi wires deformed in the transformation range [6, 13, 17, 23]. We have performed detailed TEM analysis of deformation bands observed in deformed NiTi wires: (i) in heavily deformed austenite in wide temperature and strain range [34], (ii) in cyclically deformed wires [6, 7, 13] and (iii) in wires subjected to heating under constant strain up to high temperatures [20]. The bands are important, since very large unrecoverable strain is localized in them (theoretical estimate ∼ 20% in residual martensite bands, ∼ 34% in {114} austenite twins [35]). Poliatidis et al. [17], who analysed deformation bands in large grain NiTi polycrystal by combined in-situ EBSD and SEM-DIC methods, found that as much as 30% strain is localized in the wide deformation bands containing austenite twins as well as martensite plates. Ii et al. [30] presented experimental evidence for direct spatial correlation between the lattice correspondent (20–1) martensite

twins and {114} austenite twins in the microstructure of deformed NiTi. Sittner et al. [21] explained that the deformation bands containing {114} austenite twins observed in the microstructure of NiTi wire deformed in tension at high temperatures form via B2 $\Rightarrow$ B19$'$ $\Rightarrow$ B2T transformation [27] involving (20–1) deformation twinning in the oriented B19$'$ martensite. Gao et al. [32] developed a theoretical framework that can be used to identify deformation twinning systems in the B19$'$ martensite in NiTi, the activity of which leads to unrecoverable strains.

However, in spite of these recent results, the mechanism of the localized plastic deformation in martensite, which leads to the formation of deformation bands in austenite containing {114} austenite twins, has remained unknown. Even if one accepts the idea that the (20–1) martensite twins created in the martensite transform upon unloading or heating into the {114} austenite twins [21, 30, 32], there appear questions as, e.g. why the deformation localizes on mesoscale? why there are so many slip dislocations within the twins? and what is the role of the dislocation slip in B19$'$ martensite in this process? Based on the results of systematic TEM analysis of deformed B19$'$ martensites in NiTi [35] as well as on the results from the literature [30, 33], Seiner et al. [36] analysed theoretically the (20–1) deformation twinning in the B19$'$ martensite which triggers plastic deformation of the B19$'$ martensite and proposed that the deformation mechanism responsible for the creation of deformation bands is in fact combination of deformation twinning and dislocation-based kinking in the B19$'$ martensite and called it "kwinking."

In spite of the accumulating experimental evidence on the permanent lattice defects created during thermomechanical cycling of NiTi through transformation range, we are lacking statistically relevant information on these defects and related unrecovered strains. It is not known whether same lattice defects are generated: i) in superelastic and thermal cycles, ii) during forward and reverse transformation, when the transformation proceeds at low and high stresses. As far as we are aware of, there is no systematic experimental evidence on unrecovered strains and permanent lattice defects created by the martensitic transformation in thermomechanically cycled superelastic NiTi wires, based on which the deformation processes responsible for their creation could be identified and analysed.

To fill this gap, we have decided to get back to our earlier thermomechanical loading experiments aiming at evaluation of unrecovered strains [5, 13] while evaluating systematically also the lattice defects created by cycling the NiTi wire through the transformation range. We used a carefully selected NiTi wire with completely recrystallized nanograin microstructure allowing for detailed TEM analysis of the lattice defects newly introduced into the microstructure by the thermomechanical cycling. The wire was subjected to variety of thermomechanical loading tests covering wide range of temperature/stress conditions potentially encountered in engineering applications. 10 closed-loop thermomechanical load cycles was performed to increase the probability that the observed lattice defects will be relevant for assessing the cyclic instability of thermomechanical responses. The ultimate goal was to get a better insight into the cyclic instability and functional fatigue of nanocrystalline NiTi.

Experimental Methods

Commercial superelastic NiTi wire produced by Fort Wayne Metals in cold work state (FWM #1, Ti-50.9 at. % Ni, 42% CW, diameter 0.1 mm, produced in 2011) was heat treated by electropulse method [37] to prepare NiTi wire samples with desired microstructure and properties. NiTi wires with recrystallized microstructure were prepared as follows. 50-mm-long wire segments were crimped by two steel capillaries, prestressed to $\sim$ 300 MPa, constrained at current length and subjected to the short pulse of controlled electric power (power density 160 W/mm3, pulse time 15 ms). For given cold worked wire and power density used in the heat treatment, the pulse time scales with the maximum temperature reached during the electropulse heating. Since this maximum temperature largely controls the microstructure and functional properties of the heat treated wire and we keep using the same power output in our experiments, the pulse time can be conveniently used to denote the microstructure in the wire. Hence, the wire used in this work is called "15 ms NiTi wire." It has fully recrystallized microstructure with mean grain size d = 250 nm. The wire undergoes B2-R-B19$'$ transformation upon cooling with characteristic transformation temperatures R_s = –25 °C, M_s = –80 °C, A_f = –27 °C [37], and its basic transformation and mechanical properties are summarized in Figs. 1, 2, 3, and 4.

Thermomechanical loading tests in tension were carried out using custom-made tensile tester MITTER for thin SMA wires consisting of a miniature load frame, environmental chamber, electrical conductive grips, a load cell, a linear actuator and a position sensor. The environmental chamber (Peltier elements, resistive elements and liquid nitrogen vapours) enables to maintain homogeneous temperature around the thin wire from –100 °C to 200 °C. The temperature, stress or strain are controlled and recorded by the close-loop Labview controlled system. The wire sample was gripped into the tester, strain was set to zero in the austenitic state at room temperature and the wire was heated/cooled to the desired test temperature under 20 MPa stress and tensile thermomechanical test was performed
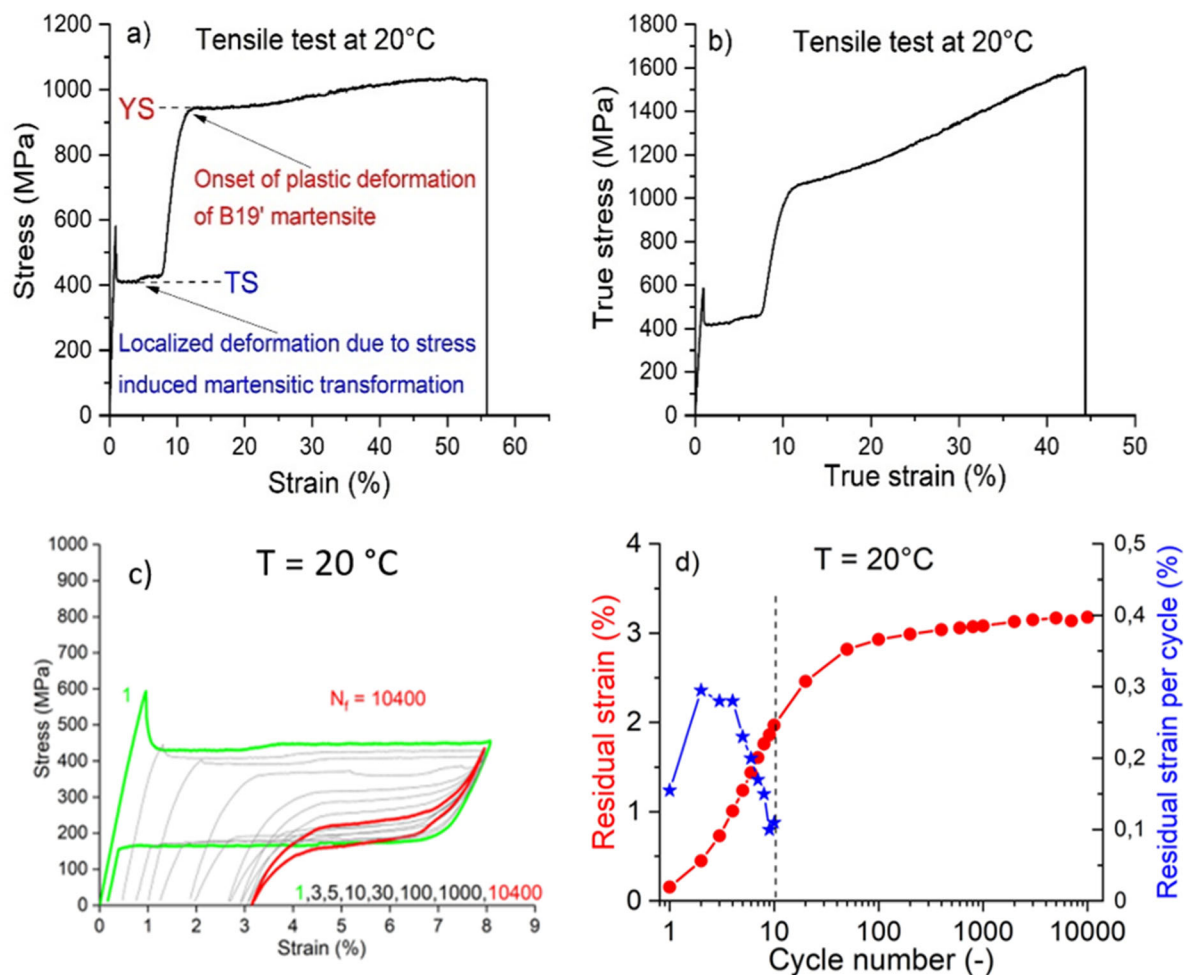
Fig. 1 Basic mechanical characteristics of 15 ms NiTi wire: **a**, **b** Tensile test at room temperature till fracture, **c** Cyclic superelastic test till failure, **d** Accumulation of residual strain upon cycling

according to the test control programme. Stress–strain–temperature–electric resistance of the wire was recorded during the whole thermomechanical loading test. Table 1 contains list of performed thermomechanical loading experiments with information on temperature and stress condition at which forward and reverse transformation take place. As each test starts and finishes in the austenite phase, we evaluated unrecovered strain (US) in each test, which is also given in Table 1.

Microstructure of wires subjected to wide range of thermomechanical loading tests was observed by Transmission Electron Microscopy (TEM). A lamella was cut from the subsurface layers of deformed wire (5 μm below the surface, wire axis in the lamella plane) by focussed ion beam (FIB) using a FEI Quanta 3D FIB-SEM microscope. The lamellae were cut with the wire axis always lying in plane. TEM observations were performed using a FEI Tecnai TF20 X-twin transmission electron microscope equipped with a field emission gun operated at 200 keV using a double-tilt specimen holder. In order to observe

lattice defects created during the thermomechanical loading tests, the microstructure of the wire (Fig. 3a) has to be free of any lattice defects observable by TEM prior the thermomechanical loading. This is the case in NiTi wires with recrystallized microstructure. Simultaneously, the grains have to be large enough so they do not overlap in the $\sim$ 70 nm thick lamella but small enough so that the wire shows stable superelasticity at least at room temperature. The 15 ms NiTi wire with small recrystallized grains $\sim$ 250 nm in diameter was intentionally selected as a compromise.

Results

The thermomechanical loading tests were carefully designed so that martensitic transformation proceeds under wide range of stresses and temperatures. Thermomechanical loading tests are described by stress–temperature paths drawn in the stress–temperature σ-T diagram denoting the
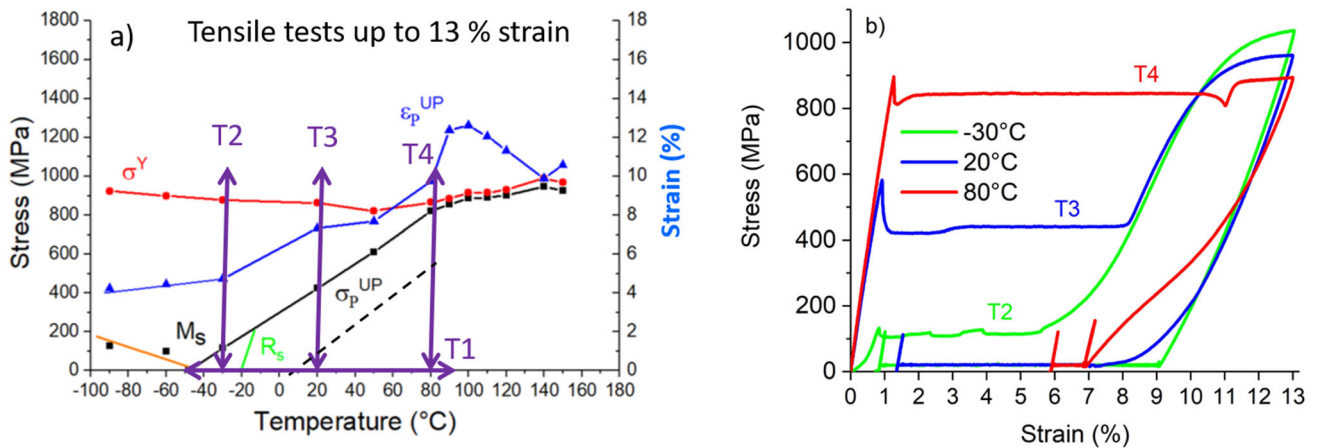
Fig. 2 **a** The stress–temperature diagram of the 15 ms NiTi wire loaded in tension taken from [37] denotes stress–temperature conditions, at which various deformation/transformation processes take place, **b** Stress–strain curves determined in thermomechanical loading tests T2–T4 (deformation at constant temperatures −30 °C, at 20 °C, and 80 °C up to 13% strain followed by unloading and heating up to 150 °C under 20 MPa stress. The σ-T diagram contains transformation lines corresponding to the forward and reverse B2-B19′ transformation (solid and dashed black), reorientation of B19′ martensite (orange), B2-R transformation (green) and the onset of plastic yielding of oriented martensite (red). The plateau strain ε_p^{UP} recorded in tensile tests increases with increasing test temperature and shows a maximum at 100 °C (blue). T1 is a stress-free electric resistivity thermal cycle across transformation range cycle (Fig. 3b). Stress–temperature path of tests T1, T2, T3 and T4 are denoted by arrows in (**a**)
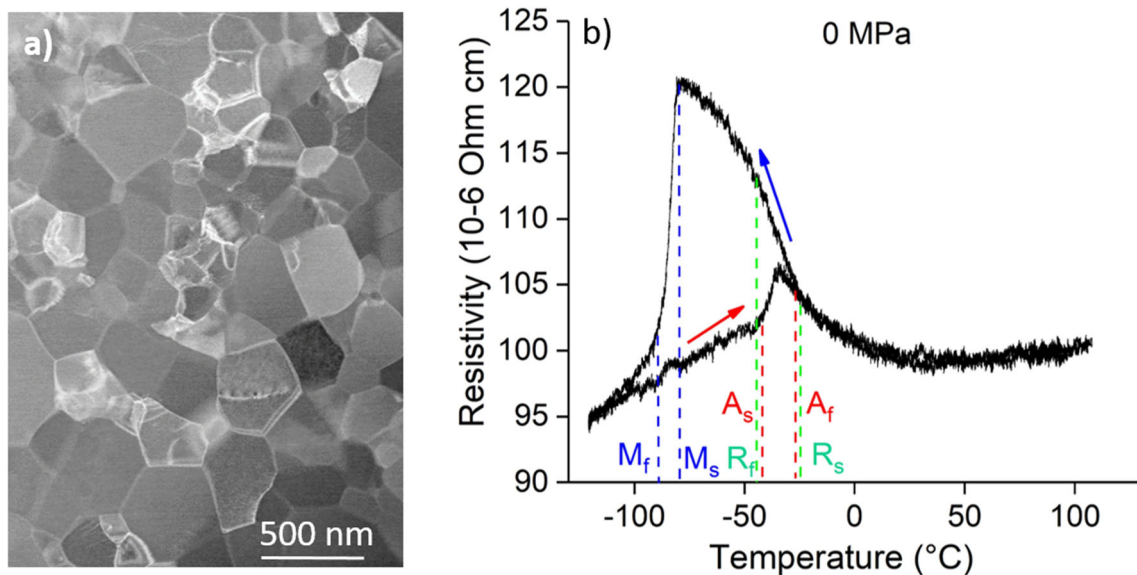

Fig. 3 **a** Microstructure of the virgin austenitic 15 ms NiTi wire. **b** Electrical resistivity thermal cycle across transformation range (test T1). There are no lattice defects observable by TEM in the recrystallized microstructure

stress–temperature conditions at which martensitic transformations take place. As stress–temperature paths are closed loops always starting from and ending in the austenite state, the tests are called closed-loop thermomechanical loading tests. The σ-T diagram of the wire is introduced in Sect. "Stress-temperature diagram". Then we present the results of conventional superelastic and actuator cycling tests (Sect. "Cyclic superelastic and thermal loading tests"), cyclic shape memory and recovery stress tests (Sect. "Cyclic shape memory and recovery stress tests") and dedicated cyclic thermomechanical loading tests allowing for the evaluation of accumulated unrecovered strains and permanent lattice defects created during the forward and reverse martensitic transformation separately (Sect. "Cyclic bypass tests separating the effects of forward and reverse transformations").
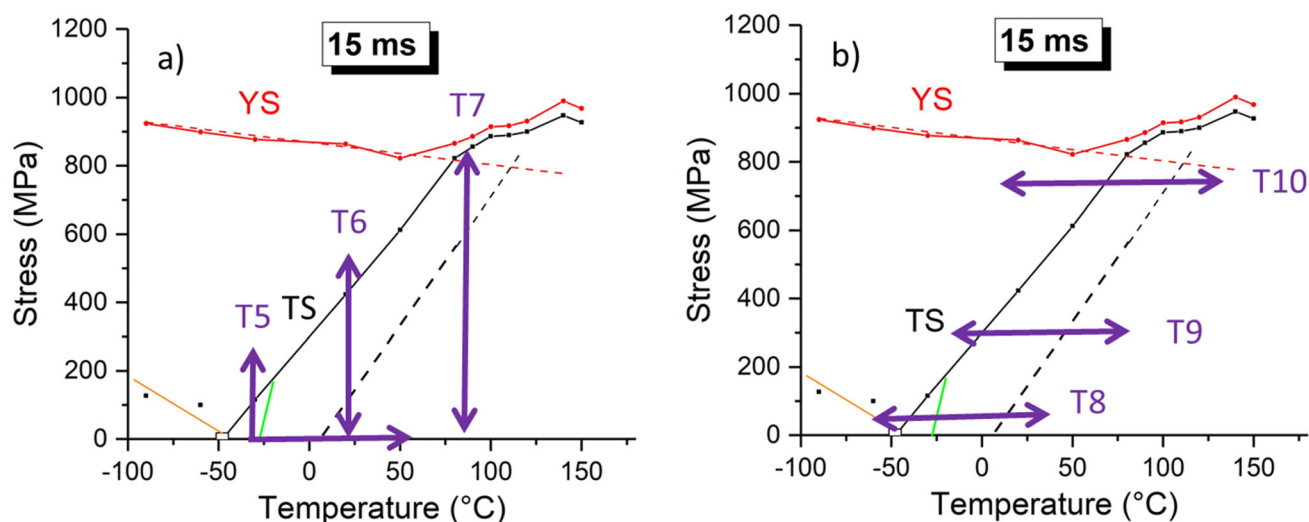
Fig. 4 Stress–temperature paths of the basic thermomechanical loading tests T5–T10 (10 cycles) denoted in the σ-T diagram include: **a** Tensile tests at constant temperatures −30 °C, 20 °C, 80 °C. **b** MPa thermal cycling at constant stresses 6.5 MPa, 280 MPa, 750 MPa. In case of the test T5, the test starts by cooling to the test temperature −30 °C, at which the wire is loaded/unloaded and, since there is large residual strain left on unloading, the test is completed by heating under small stress 20 MPa above A_f and cooling back to the room temperature

Table 1 List of thermomechanical loading tests

Test no	Description	Forward MT		Reverse MT		US
		TT [°C]	TS [MPa]	TT [°C]	TS [MPa]	10 cycles [%]
T1	Electric resistivity test	−80		−27		(1 cycle)
T2	1TeT at −30 °C up to 13% strain	−40	130	20	20	0.82 (1 cycle)
T3	1TeT at 20 °C up to 13% strain	20	450	30	20	1.33 (1 cycle)
T4	1TeT at 80 °C up to 13% strain	80	850	80	400	5.9 (1 cycle)
T5	10SMC at −30 °C	−30	170	−30	20	0,1
T6	10SEC at 20 °C	20	440	20	150	1.65
T7	10SEC at 80 °C	80	850	80	400	6.45
T8	10THC at 6.5 MPa	−65	6.5	−25	6.5	0
T9	10THC at 280 MPa	−20	280	50	280	1.93
T10	10THC at 750 MPa	45	750	130	750	20.1
T11	10SMC at 8% strain	−40	20	15	20	0.12
T12	10RSC at 7% strain	−40–80	100–500	−40–80	100–500	0.44*
T13	10SEC at 30 °C	30	500	30	200	2.45
T14	10SEC at 30 °C Forward	30	465		20	2.1
T15	10SEC at 30 °C Reverse	−40	20	30	250	1.5
T16	10THC at 400 MPa	25	400	45	400	3.7
T17	10THC at 400 MPa Forward	25	400	−5	20	0.41
T18	10THC at 400 MPa Reverse	−40	20	60	400	6.4

TT transformation temperature, *TS* transformation stress, *US* unrecovered strain, *incomplete transformation, *TeT* tensile test, *THC* thermal cycling under constant stress, *SEC* superelastic cycling at constant temperature, *SMC* shape memory cycling—thermomechanical, *RSC* recovery stress cycling – thermomechanical

Stress–Temperature Diagram

Basic results of tensile tests on 15 ms NiTi wire at room temperature until failure and cyclic superelastic tensile test until failure are presented in Fig. 1. The stress–strain curve till fracture (Fig. 1a) shows characteristic stress plateau due to the stress-induced martensitic transformation proceeding at forward transformation stress (TS) and second yielding, where plastic deformation of the stress-induced martensite process starts at the yield stress (YS). Since the 15 ms NiTi wire deforms up to ~ 55% strain until failure, true stress–true strain curve is shown in Fig. 1b to demonstrate the level of strain hardening the wire displays in the plastic deformation range beyond the yield stress. It shall be pointed that not every NiTi wire can be deformed up to ~ 55% tensile strain, in fact, most of the high-quality superelastic NiTi wires fracture at ~ 13–15% strain (see Fig. 5 in [37]).

The cyclic superelastic stress–strain curve (Fig. 1c) shows plateau type character and considerable instability upon superelastic cycling typical for nanocrystalline recrystallized NiTi wires [37]. Since the tensile deformation of the 15 ms NiTi wires is localized in transformation fronts [6, 38], it is essential that the wire was always deformed till the end of the stress plateau (i.e. that it transformed everywhere along the gauge length) but not much beyond the end of plateau, so that plastic deformation due to overloading did not take place. Under such circumstances, the recorded accumulated unrecovered strain and the observed permanent lattice defects are representative for the performed thermomechanical loading test.

Since the goal was to investigate the cyclic instability of the NiTi wire, there was an additional requirement on the wire to be used in experiments—it had to display considerable cyclic instability and accumulation of unrecovered strains in 10 cycles, Typical high-quality superelastic NiTi wires used in in engineering applications display minor instability spreading over thousands of cycles. The selected 15 ms NiTi wire was a compromise also from this point of view. Although the residual strain recorded in the first cycle (Fig. 1c, d) is rather small, there is more than 3% of residual strain accumulated after 10,400 cycles in the cyclic superelastic test at 20 °C. Maximum residual strain (and presumably lattice defects) are generated in the 2–5th cycle, not in the 1st cycle (Fig. 1d). Most of the residual strain is accumulated in the first ~ 30 cycles, as can be read from Fig. 1d showing also how accumulated residual strain evolves with increasing number of cycles. It shall be pointed out that this scenario drastically varies with the test temperature [39] and type of the test. Hence, we have decided to evaluate unrecovered strains and permanent lattice defects after 10 closed-loop thermomechanical
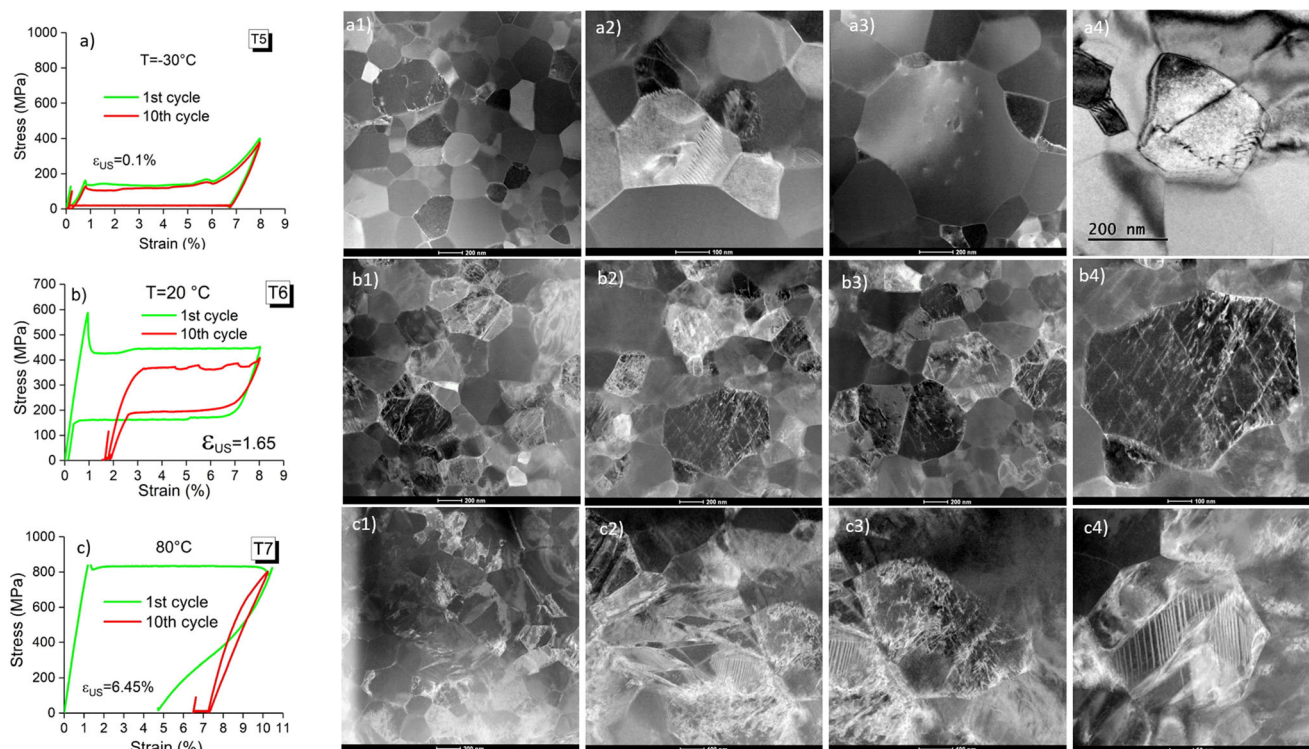

Fig. 5 Cyclic tensile tests at constant temperature T5–T7. Stress–strain curves recorded in the 1st and 10th cycle and lattice defects observed in the microstructure of the cycled wires (10 closed-loop cycles followed by heating to 150 °C)

loading cycles, since we believed that this is a reasonable compromise for the 15 ms NiTi wire.

Stress-free cooling/heating across transformation temperature interval in electric resistivity thermal cycle (test T1) was performed to determine transformation temperatures of the wire transforming in the absence of tensile stress (Fig. 3b, Table 1). The wire clearly undergoes two step B2 = > R = > B19′ martensitic transformation upon cooling and partially also upon heating. When even very small stress was applied (as e.g. in the dilatometer test T8 in (Fig. 6a)), M_s temperature shifts upwards, A_f temperature remains unchanged and single-step B19′ = > B2 transformation occurs upon heating.

Stress–temperature σ-T diagram determined for the 15 ms NiTi wire in our earlier work (Fig. 8c in [37]) is reproduced in Fig. 2a. Stress–temperature conditions, at which forward (σ_p^{UP}) and reverse (σ_p^{LO}) martensitic transformations take place in this wire, are denoted by transformation lines in the σ-T diagram (solid and dashed black curves in Fig. 2a). Temperature dependence of the yield stress σ^Y, at which plastic deformation of martensite starts (red curve in Fig. 2a), is denoted in the diagram as well as the temperature dependence of the plateau strain ε_p^{UP} recorded in the tensile tests (blue curve in Fig. 2a). See article [6] for the analysis of the plateau strain ε_p^{UP} increasing with increasing temperature and article [34] for

analysis of unrecovered strain recorded in tensile tests up to large deformations at various test temperatures. The results of three tensile tests T2,T3,T4 performed intentionally up to 13% strain to determine the values of σ^Y at three different temperatures are shown in Fig. 2b.

Since the terms "residual strain", "unrecovered strains" and "permanent lattice defects" are used throughout this work with specific meanings, possibly different from the intuitively understood meanings, let us briefly comment on this. The "residual strain" is the strain determined on the stress–strain curve or strain—temperature curve after loading/unloading or cooling/heating, respectively. When the wire is subsequently heated far above the A_f temperature, reverse martensitic transformation of the residual martensite is activated and part of this residual strain is recovered. The plastic strain which remains after this final heating of the wire far above the A_f temperature is called "unrecovered strain" and lattice defects observed in the austenitic microstructure are called "permanent lattice defects". There could be small or large differences between the residual and unrecovered strains (compare for example the results of the tests T2 and T4 in Fig. 2b).

Knowing the stress–temperature diagram for the 15 ms NiTi wire, we planned and carried out series of thermomechanical loading tests consisting in 10 closed-loop thermomechanical loading cycles along various paths in
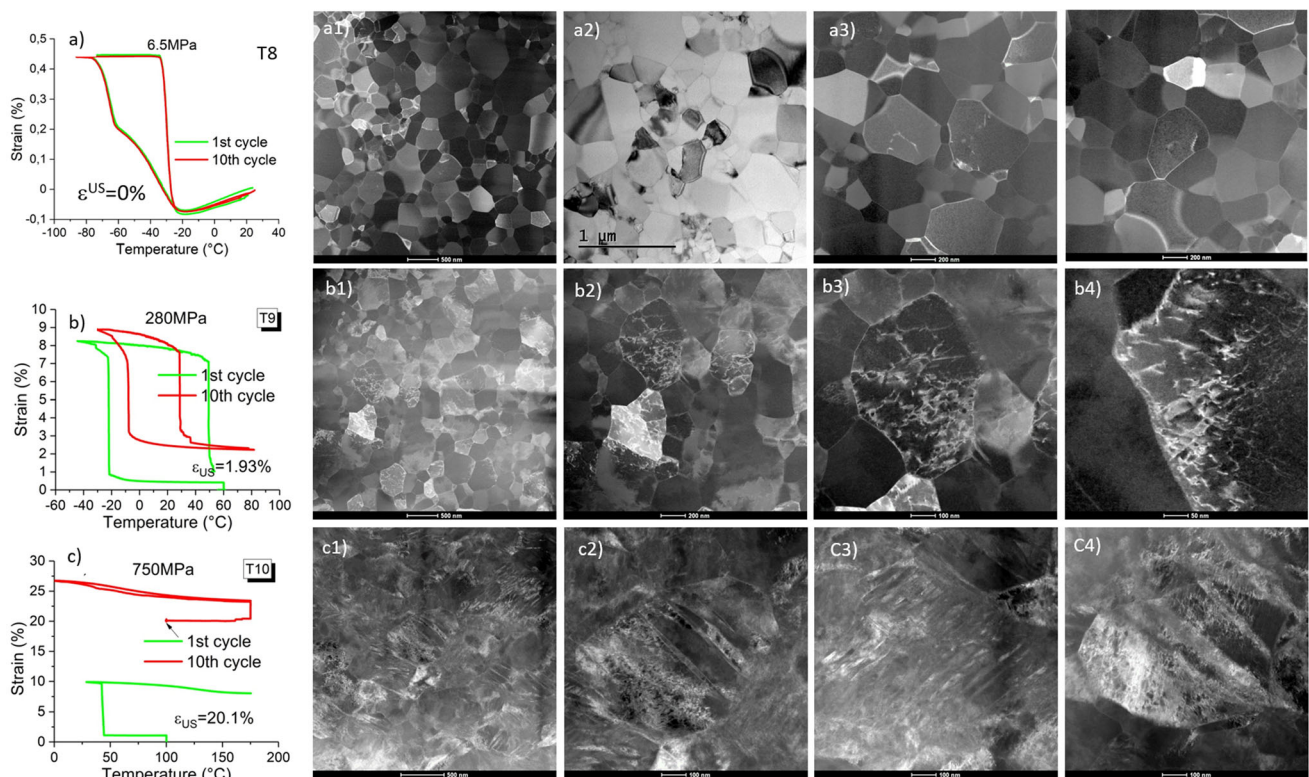

Fig. 6 Cyclic thermal loading at constant stress T8–T10. Strain–temperature curves recorded in the 1st and 10th cycle and lattice defects observed in the microstructure of the cycled wires (10 closed–loop cycles followed by heating to 150 °C)

the stress–temperature space (T5–T18 in Table 1). The tests are organised in groups, the results of which are presented in Sects. "Cyclic superelastic and thermal loading tests", "Cyclic shape memory and recovery stress tests", "Cyclic bypass tests separating the effects of forward and reverse transformations". To guide the reader through the relatively complex thermomechanical loading tests, the stress–temperature paths of these tests are presented in the σ-T diagram. The relevant stress–strain–temperature responses recorded in the 1st and 10th cycle are shown to characterize the stability/instability of the cyclic functional response of the wire. For each test, values of TT and TS for forward and reverse martensitic transformation and unrecovered strains recorded in the test are presented in Table 1.

Cyclic Superelastic and Thermal Loading Tests

Series of cyclic superelastic test at constant temperature (Fig. 4a) and thermal cycling at constant stress (Fig. 4b) were performed to evaluate unrecovered strain and permanent lattice defects generated by martensitic transformation proceeding under very different stress–temperature conditions. Since the superelastic strains in tensile test at T = −25 °C (T5) are not recovered upon unloading (Fig. 5a), the closed-loop thermomechanical loading cycle was completed by heating under 20 MPa stress (Figs. 4a, 5a). The superelastic test T6 and actuator test T9 are basic tests used to investigate functional thermomechanical properties of NiTi wires. The results of these tests are compared with the results of tests T5, T8 (T7, T10), for which the martensitic transformation proceeds at lower (higher) stresses and temperatures, respectively. The unrecovered strains recorded in the tests are listed in Table 1 and the permanent lattice defects generated upon cycling are shown in Figs. 5 and 6.

Superelastic tensile test at room temperature (T6 in Fig. 5b) generates medium unrecovered strain 1.65%, significant amount of slip dislocations and only few deformation bands containing residual B19′ martensite or {114} austenite twins. The reader is referred to our related paper [13], in which these slip dislocations were analysed as belonging to the $\{011\}/<100>$ austenite slip system. The stress–strain response in the test T6 was unstable, hysteresis width decreased due to the gradual decrease of the upper plateau stress in 10 cycles. This contrasts with the test T5 at −30 °C (Fig. 5a), in which only negligible unrecovered strain and few scattered dislocation segments were observed in the microstructure of the cycled wire and very good cyclic stability of the stress–strain–temperature response of the wire was observed In this test, the forward martensitic transformation proceeds from the R-phase into the B19′ martensite at low stress ∼ 100 MPa while the reverse transformation takes place upon heating under

20 MPa. Although the maximum stresses, strains and temperature applied in tests T5 and T6 were comparable, the forward and reverse martensitic transformations proceeded at much higher stress in the latter (Fig. 4a). In the test T7 at 80 °C, the recorded cyclic stress–strain response of the wire was very unstable (Fig. 5c). Unrecovered strain reached 6.45% and stress–strain curve became almost linear with small hysteresis after 10 loading cycles. The microstructure of cycled wire is dominated by deformation bands (Fig. 5c). Detailed analysis of deformation bands created by tensile cycling of 16 ms NiTi wire deformed superelastically at elevated temperatures have shown that the bands contain either residual B19′ martensite or {114} austenite twins [7].

In the thermal cycling under constant stress 280 MPa (T9, Figs. 4b, 6b), slightly larger unrecovered strain 1.93% was observed compared to the superelastic test at 20 °C. Significant amount of slip dislocations but no deformation bands were observed in the microstructure after 10 cycles. The strain–temperature response was unstable and hysteresis width decreased significantly upon cycling, similarly as in the superelastic test at room temperature. This contrasts with the very stable strain–temperature response of the wire thermally cycled at 6.5 MPa (50 mN force) (T8, Figs. 4b, 6a). Practically no unrecovered strain was recorded, and no lattice defects were found in the wire microstructure after 10 cycles. This result, although it seems to be trivial, is very important. There are reports in the literature showing various kinds of dislocation defects created upon stress-free thermal cycling of NiTi across range of transformation temperatures M_f-A_f [11, 40], which gives an impression that cyclic martensitic transformation proceeding even without external stress generates dislocation defects in the austenite lattice. Although this might be true as concerns point defects or faults [40] (difficult to resolve by conventional TEM), our results clearly prove that no slip dislocations, twins or other lattice defects easily observable by TEM were created during the first 10 thermal cycles at low stress 6.5 MPa. The most likely explanation of this contradiction is that the literature studies were typically performed on solution-treated NiTi alloys, while our experiments were performed on superelastic NiTi wire possessing nanograin microstructure. Upon thermal cycling at 750 MPa (T10, Figs. 4b, 6c), strain–temperature response was very unstable of the ratchetting character, accumulated unrecovered strain 20.1% reached far into the plastic deformation range (Fig. 1) and very high amount of deformation bands and slip dislocations were found in the microstructure of the wire. It shall be pointed out that while the reverse martensitic transformation proceeded upon heating under stress (Fig. 6c), the wire almost did not shorten. We have investigated and analysed these ratchetting stress–strain–temperature responses upon

thermal cycling of NiTi wire under large stress in [20, 41]. The reader is referred to these articles for detailed explanation and interpretation of the ratchetting phenomenon.

Cyclic Shape Memory and Recovery Stress Tests

Results of experiments reported in Sect. "Cyclic superelastic and thermal loading tests" suggest that the stress and temperature, at which the martensitic transformation proceeds, plays a key role in the mechanism generating the unrecovered strain and permanent lattice defects. This in turn implies that the stresses and temperature applied to the wire when it does not transform are less important. In order to prove that beyond any doubts, we have performed two thermomechanical loading experiments involving high stresses and temperatures, but the martensitic transformation in them never massively proceeds at high stresses and temperatures.

First experiment is the cyclic shape memory test T11 (Figs. 7a, 8). The wire was loaded at –75 °C up to 400 MPa (8% strain), unloaded and subsequently heated under 20 MPa stress up to 20 °C. The large strain induced in the martensite state recovered almost completely during the reverse transformation on heating in each cycle. The wire displayed stable stress–strain–temperature response, small unrecovered strain 0.12% and negligible amount of permanent lattice defects (mainly dislocation segments and loops) was generated in the 10 shape memory cycles.

It has been empirically known that, in order to use NiTi elements in shape memory cycles multiple times, they have to be deformed below the M_S temperature in the low-temperature martensite state. It has been implicitly assumed that the element accumulates more damage when

it is deformed above Ms because of the higher stress, though reliable experimental evidence is lacking. Up to the author's knowledge, experimental data on the stability of cyclic shape memory effect are not available in the literature. Results published in the literature (as e.g. [42]) were typically obtained on soft NiTi alloys [42] and were limited to few tens or hundreds of cycles.

Second experiment is the cyclic recovery stress test T12 (Figs. 7b and 9). The wire was loaded at –75 °C up to 400 MPa (8% strain), unloaded to 100 MPa (7% strain) and subsequently thermally cycled under constant strain between 100 MPa and 500 MPa. Note that, although the stresses, strains and temperature involved are rather large, the martensitic transformation does not massively occur upon thermal cycling (variation of phase fraction is negligible [43]). The stress–temperature response upon thermal cycling is stable, unrecovered strain is small (0.44%) and only low density of dislocation defects (no deformation bands) was observed in the microstructure of the wire after 10 thermal cycles.

Cyclic Bypass Tests Separating the Effects of Forward and Reverse Transformations

We knew from the results of [5] that the unrecovered strains generated by the forward and reverse martensitic transformation are generally different. Obviously, this cannot be analysed based on the results of the closed-loop cyclic tests T5–T12. This section presents results of thermomechanical loading experiments T13–T15 (Figs. 10a and 11) and T16–T18 (Figs. 10b and 12) designed to evaluate the unrecovered strains and permanent lattice
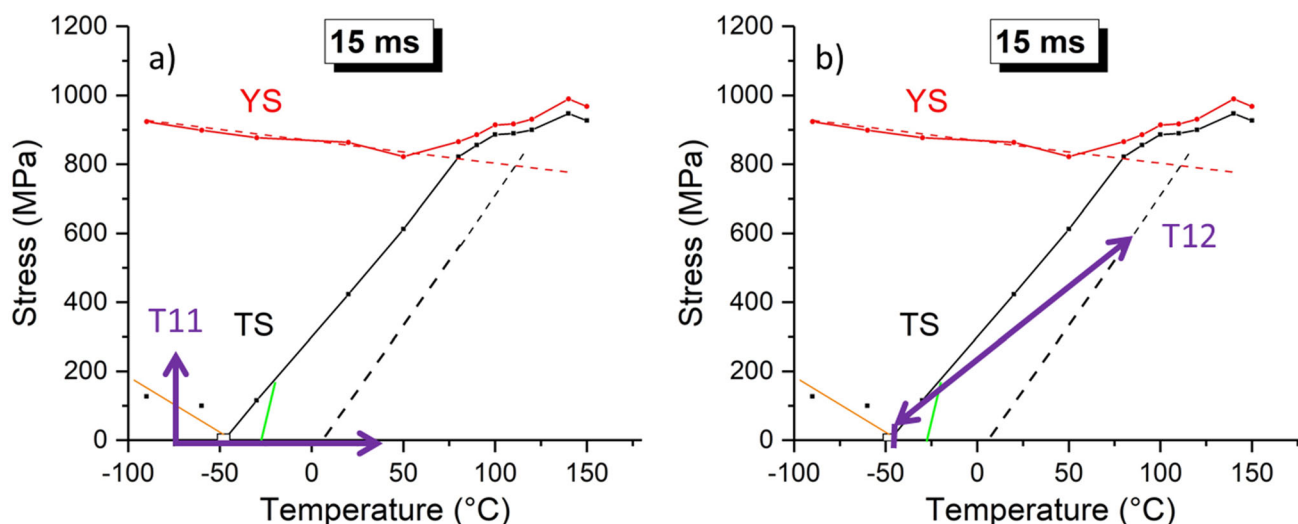

Fig. 7 Stress–temperature paths of more complex thermomechanical loading tests T11, T12 (10 cycles) include **a** Cyclic shape memory test T11 and **b** Cyclic recovery stress test T12
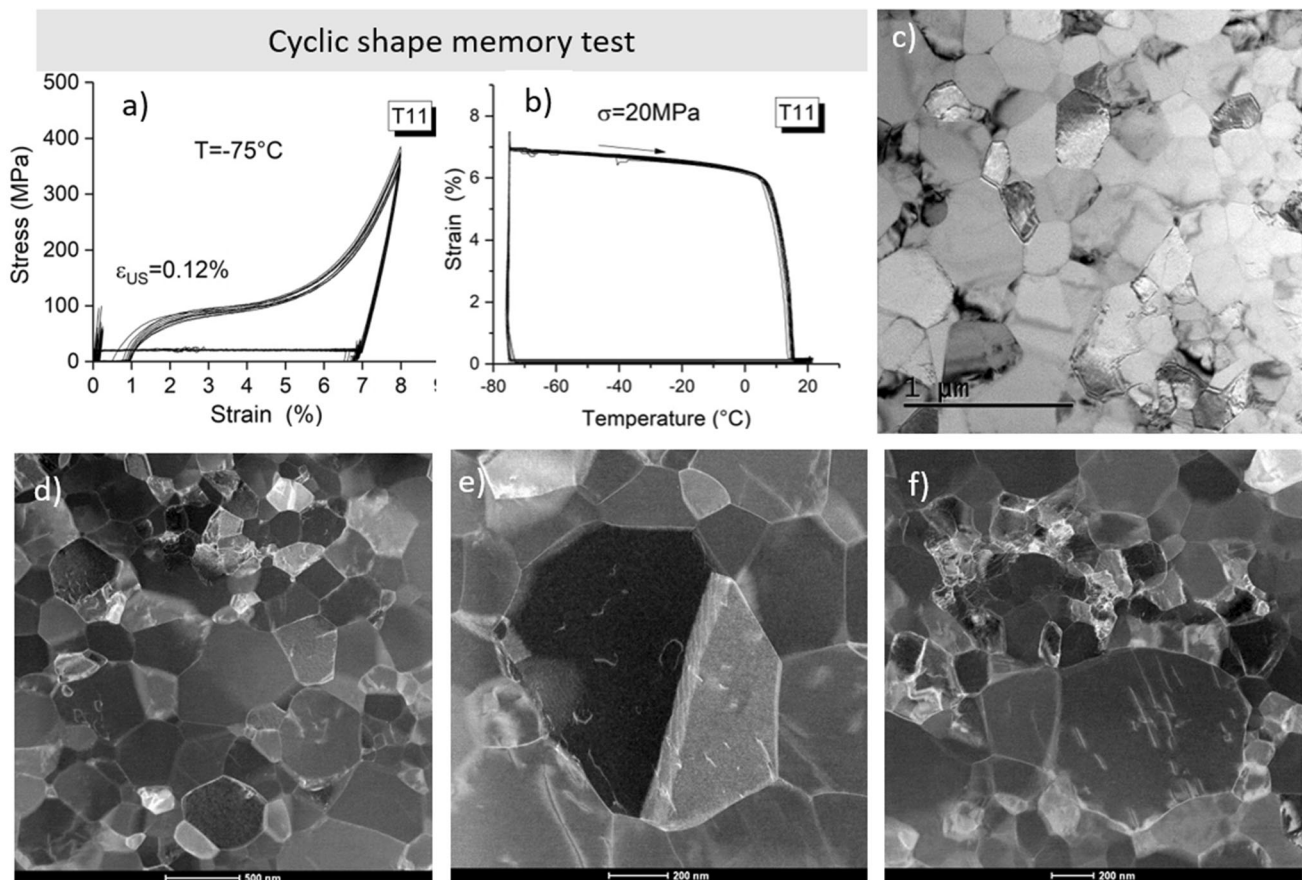
Fig. 8 Shape memory cycling T11. Stress–strain–temperature curves recorded in the first 10 cycles and lattice defects observed in the microstructure of the cycled wire (10 closed-loop thermomechanical cycles followed by heating to 150 °C)

defects created upon cycling during the forward and reverse transformations, separately.

The conventional cyclic superelastic test T13 (Figs. 10a and 11a) was performed at temperature T = 30 °C (slightly higher compared to the test T6 performed at T = 20 °C (Fig. 5b)), since we wanted higher density of lattice defects to be generated upon cycling. The recorded accumulated unrecovered strain (2.5%) is larger compared to 1.65% strain in the test T6 (Fig. 5b), and there appear deformation bands in the microstructure of the wire cycled at T = 30 °C. One cannot know from the results of the cyclic superelastic test T13 how much of the unrecovered strain was generated during the forward loading and during the reverse unloading branches of the superelastic curve. To find that, bypass thermomechanical loading tests T14 (Fig. 11b) and T15 (Fig. 11c) were performed.

In the test T14, the forward martensitic transformation upon loading at 30 °C proceeded exactly in the same manner as in the test T13, but then, instead of unloading, the wire was cooled under constant strain down to −50 °C, unloaded and heated under 20 MPa stress back to the 30 °C temperature. Such closed-loop thermomechanical loading cycle (green path in Fig. 10a) was run 10 times.

Unrecovered strain ∼ 2% was recorded after 10 thermomechanical loading cycles. When thermomechanical loading test was performed along the same stress–temperature route but counterclockwise (orange path in Fig. 10a), similar unrecovered strain ∼ 2% was determined in the test T15 (Fig. 11c). Since no unrecovered strains were assumed to be generated when the martensitic transformation proceeded under the low stress 20 MPa upon heating in the test T14 and upon cooling in the test T15, the recorded unrecovered strains and permanent lattice defects evaluated in tests T14 and T15 were assumed to be generated when the martensitic transformation proceeded under large stress upon the forward loading in the test T14 (reverse unloading in the test T15), respectively. The analysis of microstructures in wires subjected to tests T14 (Fig. 11b) and T15 (Fig. 11c) showed that there is less slip dislocations and less deformation bands in both microstructures, compared to the superelastically cycled wire T13 (Fig. 11a). Although both microstructures look quite similar, long slip dislocations appear preferentially in the forward microstructure (Fig. 11b).

The conventional cyclic thermal test T16 was performed under 400 MPa stress. In comparison to the similar test T6
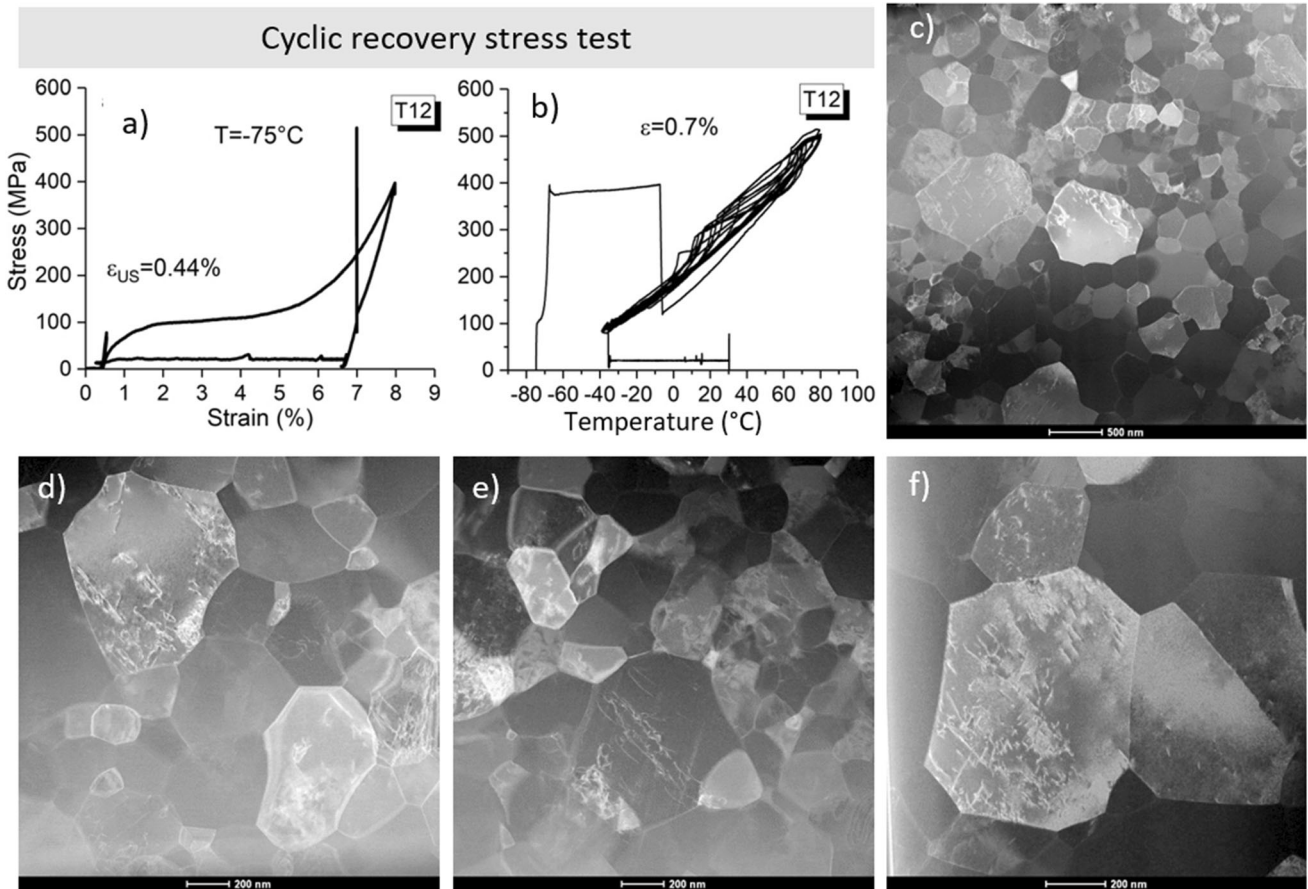
Fig. 9 Recovery stress cycling T12. Stress–strain–temperature curves recorded in the first 10 cycles and lattice defects observed in the microstructure of the cycled wire (10 closed-loop thermomechanical cycles followed by heating to 150 °C)
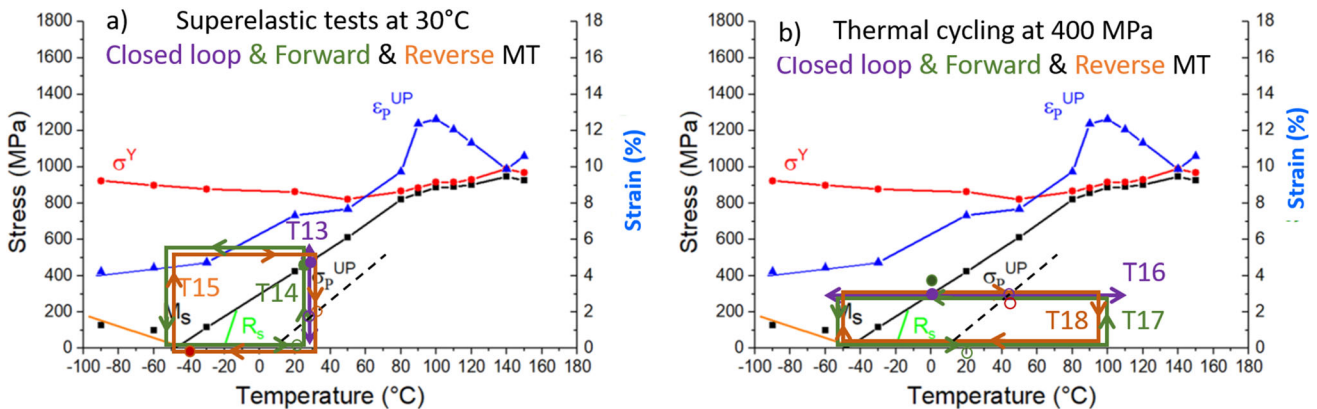

Fig. 10 Stress–temperature paths of thermomechanical loading tests T13–T18 designed to evaluate unrecovered strains and lattice defects generated separately by the forward and reverse martensitic transformations during: **a** Cyclic superelastic test T13–T15 and **b** Thermal cycling under constant stress T16–T18

performed under smaller stress 280 MPa (Fig. 6b), the accumulated unrecovered strain is significantly larger (3.7% vs. 1.93%), and there are more deformation bands in the microstructure of the cycled wire (Fig. 12a). The

hysteresis width gets narrower in similar extent as in the test T6 (Fig. 6b) but, in a contrast, the decrease of the hysteresis width is mainly due to the shift of the reverse transformation to lower temperatures. Again, we did not
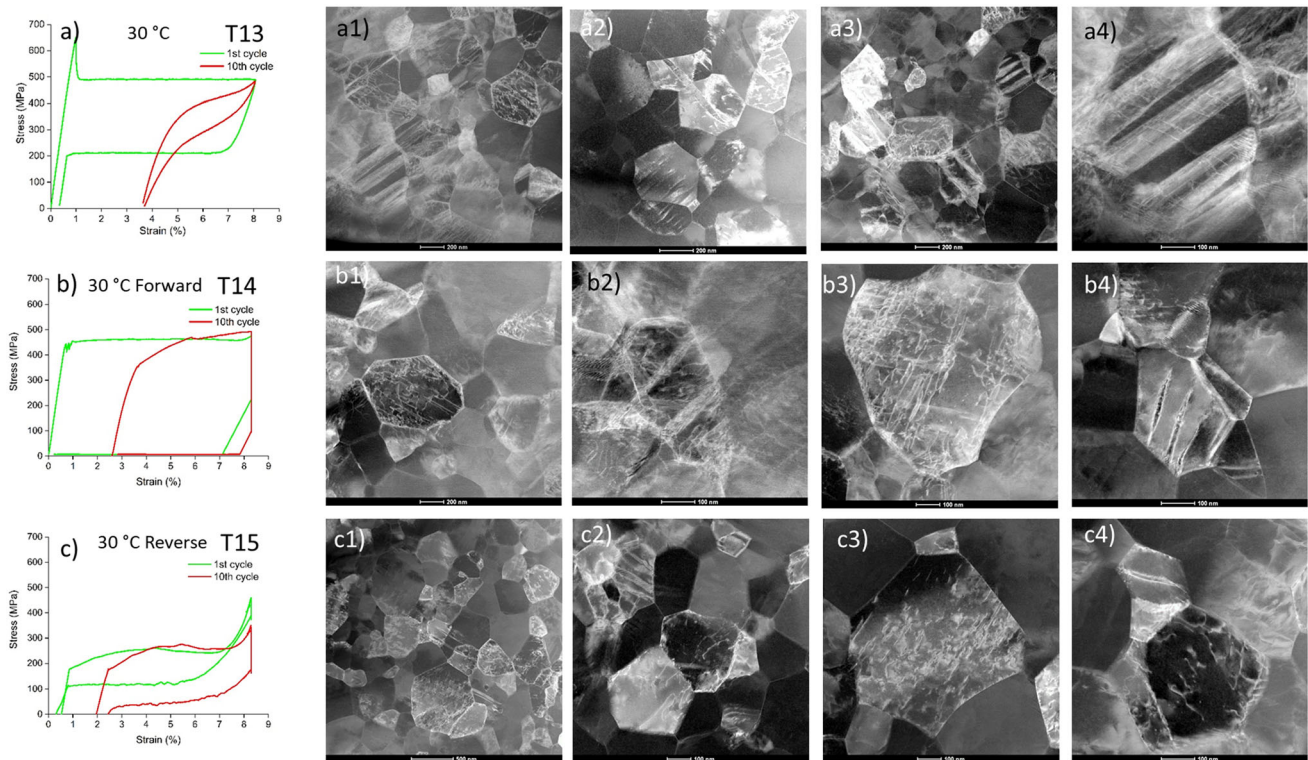
Fig. 11 Thermomechanical loading tests T13–T15 performed to evaluate unrecovered strains and lattice defects generated separately by the forward (T14) and reverse (T15) martensitic transformation in superelastic test (T13). Stress–strain curves recorded in the 1st and 10th cycle in thermomechanical loading tests and lattice defects observed in the microstructure of the cycled wires (10 closed-loop cycles followed by heating to 150 °C)

know from the test T16, how much of unrecovered strain and lattice defects was generated during the forward cooling and reverse heating. The bypass thermomechanical loading tests T17 (green path in Fig. 10b) and T18 (orange path in Fig. 10b) were performed to find out that. While only very small unrecovered strain 0.41% was recorded in the test T17 (Fig. 12b), in which the martensitic transformation proceeded under stress only during the forward cooling, very large unrecovered strain 6.4% was recorded in the test T18 (Fig. 12c), in which the martensitic transformation proceeded under the same stress only during the reverse heating. The microstructures observed in the cycled wires (Fig. 12b, c) are in agreement with the difference in unrecovered strains. It appears that the permanent lattice defects (slip dislocations and deformation bands) were generated mainly during the reverse heating under stress. The unrecovered strain and amount of lattice defects generated in the test T18 (cyclic reverse transformation under stress) are even much higher than that in the test T16 (conventional cyclic thermal test under 400 MPa).

Discussion

Based on the presented results, it appears that plastic deformation occurs (unrecovered strains and permanent lattice defects are generated) during the thermomechanical cycling of NiTi wire only if the martensitic transformation proceeds under elevated external stress (i.e. not when the wire transforms under low stress, when it is deformed in the low-temperature martensite state or when it is loaded elastically even to very high stresses at high temperatures in the austenite state). This is the key result of this work. Concerning the unrecovered strain, this was the main conclusion of our previous work [5] but very little was known about the permanent lattice defects.

Of course, this conclusion applies only for NiTi wires deformed within the transformation range. If the wire is deformed plastically beyond the crystallographic limits of the B2-B19′ transformation, as e.g. in the tests T2–T4 (Fig. 2), plastic deformation proceeds within the martensite phase and lattice defects created in the martensite are inherited into the austenitic microstructure upon the reverse martensitic transformation [35, 34]. This is, however, out of the scope in this work. Large deformations were avoided
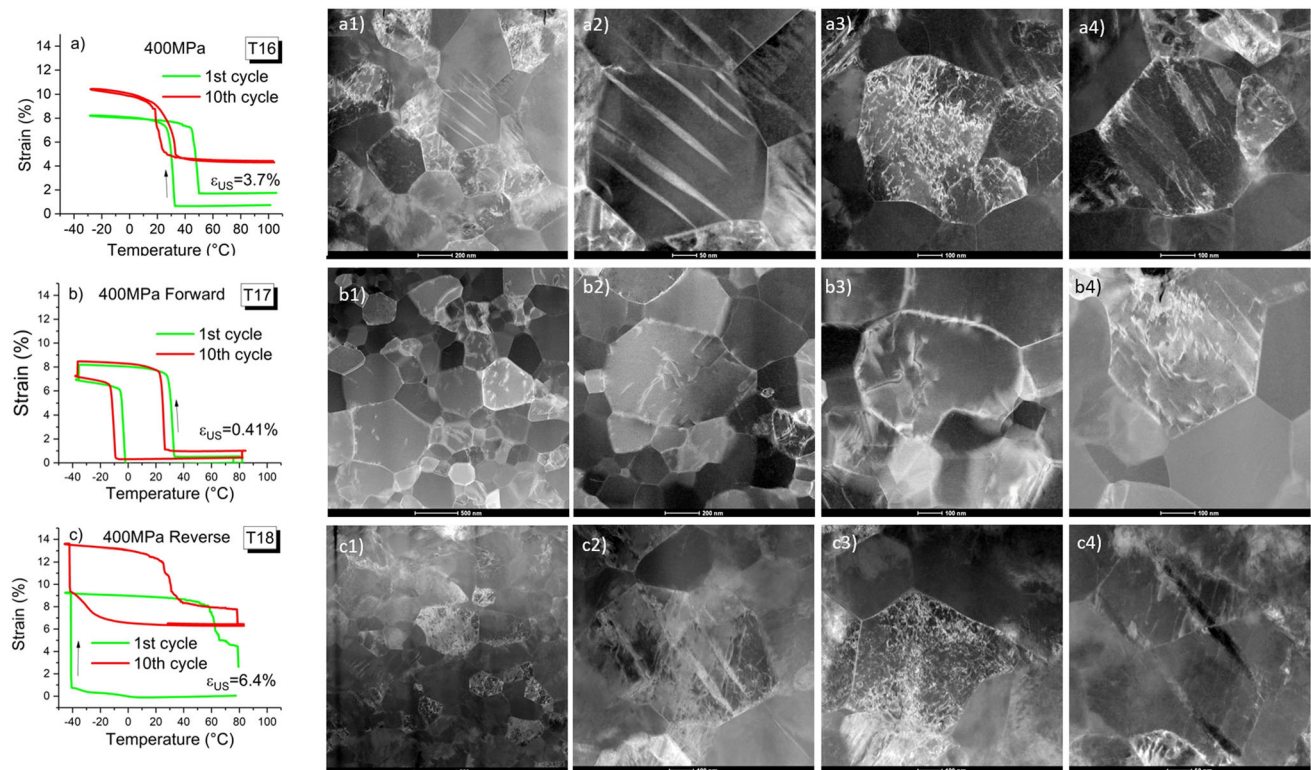
Fig. 12 Thermomechanical loading tests T16–T18 performed to evaluate unrecovered strains and lattice defects generated separately by the forward (T17) and reverse (T18) martensitic transformations in thermal cycling under constant stress (T16). Stress–strain curves recorded in the 1st and 10th cycle in thermomechanical loading tests and lattice defects observed in the microstructure of the cycled wires (10 closed-loop cycles followed by heating to 150 °C)

in all tests, with the exception of the ratchetting strain–temperature response in the test T10.

With respect to similar experiments in [5], the thermomechanical loading experiments T5–T18 were performed with three important innovations: (1) the experiments were performed on recrystallized NiTi wire with suitable grain size so that permanent lattice defects created in the virgin austenitic microstructure upon cycling can be observed and analysed, (2) the type of experiments was carefully selected to cover whole range of stress, temperature conditions at which the martensitic transformations may proceed in real applications, (3) 10 thermomechanical cycles were performed instead of one cycle only (this is important since deformation bands are promoted by cycling).

In following section, we discuss the experimental evidence suggesting that even the 15 ms NiTi wire with recrystallized microstructure may potentially show very stable stress–strain–temperature responses in cyclic thermomechanical loads under specific conditions. In further sections, we discuss the observed lattice defects (Sect. "Permanent lattice defects"), the generation of unrecovered strains and permanent lattice defects in thermomechanically cycled NiTi wire in dependence on the stresses/temperatures at which martensitic transformation proceeds (Sect. "The effect of temperature/stress at which the forward and reverse martensitic transformation takes place") and the effect of the virgin austenitic microstructure of the wire on the cyclic instability (Sect. "The effect of virgin austenitic microstructure").

Stable Functional Responses

Considering that unrecovered strains are generated only if martensitic transformation proceeds under elevated external stress, questions appear whether and in which thermomechanical loading tests a particular NiTi wire can be used without generating unrecovered strains and lattice defects. We have reported above that marginal unrecovered strains and only very few permanent lattice defects were generated in cyclic thermomechanical loading tests in which:

(i)   martensitic transformation proceeded under very small stress (T5, T8),

(ii)   no transformation proceeded under stress in cyclic shape memory test T11,

(iii)   the martensitic transformation proceeded only marginally upon thermal cycling in cyclic recovery stress test T12.

The observed stress–strain–temperature responses in all these tests were found to be very stable, in spite of the large stresses, strains and temperatures applied in some of these tests. This observation is very important, since it apparently contradicts results of many literature reports, in which massive dislocation generation in transforming NiTi was observed upon stress-free thermal cycling [11], martensite reorientation by deformation [44, 45] or martensitic transformation proceeding under relatively low applied stress [13, 17].

The problem is that the NiTi alloys used in these experiments were frequently either solution-treated or annealed alloys, which were simply too soft to show stable functional behaviours at all. The solution-treated NiTi single crystals and polycrystals show in many respects different properties from the nanocrystalline NiTi wires studied in this work. Two most important differences are that (i) the solution-treated alloys have very low-yield stress for plastic deformation and (ii) martensitic transformation upon stress-free cycling proceeds via propagation of habit plane interphases between B2 austenite and type-II twinned martensite interfaces [1]. In a contrast, the NiTi wires with nanocrystalline microstructure are highly resistant to plastic deformation in martensite [5], and the microstructure of thermally induced martensite is formed by (001) compound twins [46, 47, 35].

The results of tests T5, T8, T11 and T12 clearly show that martensitic transformation may proceed in thermo-mechanically cycled nanocrystalline NiTi wire without generating unrecovered strains and permanent lattice defects observable by conventional TEM. This allows for stable stress–strain–temperature responses in thermomechanical loading test under specific conditions. High-cycle thermomechanical loading tests to determine the functional fatigue of such wires yet remain to be performed.

Permanent Lattice Defects

Since the martensitic transformation, in theory, does not leave behind any lattice defects, the permanent lattice defects observed in the microstructure of deformed wires are considered to be relicts of the plastic deformation processes that potentially accompanied the cyclic martensitic transformation during the closed-loop cycling. In other words, if an incremental plastic deformation occurred within the cycled wire, we shall evaluate unrecovered strain and we might observe permanent lattice defects in the austenitic microstructure of the cycled wire. If it did not occur, we shall see no unrecovered strains and shall not find any new permanent lattice defects in the microstructure of cycled wires.

We have performed 10 thermomechanical loading cycles to increase the probability that the observed type and density of lattice defects are statistically representative for the martensitic transformation taking place under given stress/temperature conditions. To provide the reader with relevant experimental information on the observed defects, we used STEM mode, in which dislocation defects, austenite twins and deformation bands are better highlighted in large number of variously oriented grains within one micrograph while the disrupting contrast on bending contours is suppressed. We did not analyse the observed lattice defects in detail in this work, since we did that and reported before, particularly to the slip dislocations [13], residual martensite bands [7] and austenite twins [6].

The permanent lattice defects observed by TEM in the microstructure of NiTi wires subjected to 10 thermomechanical loading cycles are

(i)   **dislocation loops and isolated dislocation segments** observed in tests, in which martensitic transformation proceeds at very low stresses and temperatures (T1, T5, T8, T11)

(ii)   **(110)/ < 001 > slip dislocations a**t intermediate stresses and temperatures (T6, T9, T12, T13, T14, T15, T17)

(iii)   **deformation bands** containing typically {114} austenite twins with high density of unidentified slip dislocations both inside the twins and surrounding matrix at high stresses and temperatures (T7, T10, T13, T14, T15, T16, T18)

The type of the observed permanent lattice defects depends mainly on the stresses/temperatures, at which the forward and/or reverse martensitic transformation proceeded in the test. Based on the results of conventional thermomechanical tests T5–T13, T16, in which both forward and reverse martensitic transformations proceeded under elevated stress, we cannot specify whether the observed lattice defects were created during the forward or reverse martensitic transformation (Fig. 13). This can be determined from the results of the bypass test T14, T15, T17, T18, in which either forward or reverse transformation is bypassed (proceeds 10 times at very low stress ∼ 20 MPa), and hence, the observed lattice defects can be ascribed to the plastic deformation accompanying the forward or the reverse martensitic transformation proceeding under elevated stress (>100 MPa). Generation of unrecovered strains by the forward and reverse martensitic transformations in dependence on the temperature and stress at which it proceeded is discussed with the help of Fig. 14. The unrecovered strain and type of lattice defects
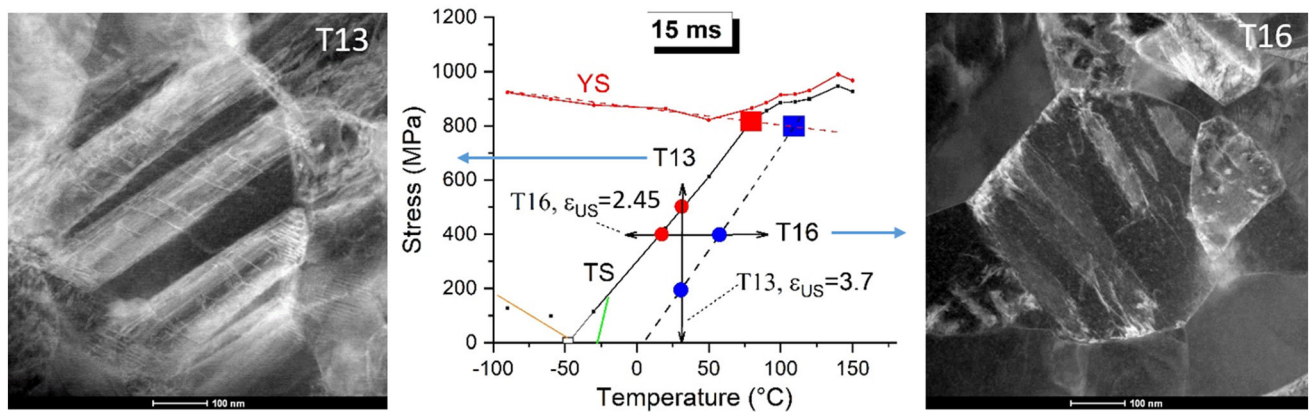
Fig. 13 Unrecovered strain and lattice defects generated in 10 superelastic cycles at room temperature (T13) and thermal cycling under 400 MPa (T16). Lattice defects generated by superelastic cycling and thermal cycling under stress are rather similar, deformation bands as well as slip dislocations appear in both tests. Whether they were created during the forward and/or reverse martensitic transformations cannot be determined from these conventional tests

generated under various stresses and temperatures are summarized in Fig. 15.

Isolated dislocation loops and segments were observed in the austenitic microstructure after thermal cycling under lowest stresses 6.5 MPa in the test T8 (Fig. 6a). The recorded strain–temperature response was stable and hysteresis width was about 40 K. The thermally induced martensite in this nanocrystalline wire is formed by domains of (001) compound twinned B19′ martensite [35] which form via R-phase (Figs. 3b and 6a), reorient upon tensile deformation into single domain martensite [35] and reverse transform back into parent austenite upon stress-free heating during the shape memory cycle. Since the forward and reverse martensitic transformations in these tests proceed in the absence of stress, very small unrecovered strains, very few permanent lattice defects and no deformation bands were generated upon cycling.

The compound twinned martensite in nanograined NiTi was analysed in detail in series of articles by Waitz [46–48]. He argued that the B2 austenite in nanograined NiTi transforms upon cooling into single- or multiple-compound-twinned domains of B19′ martensite because of the energy reasons [48]. Our results [35] show that this is the case also for the 15 ms NiTi wire with significantly larger mean grain size ~ 250 nm. Anyway, there must exist a mobile interface between the B2 austenite (R-phase) and the B19′ martensite, which propagates cyclically under low stress without generating unrecovered strain and lattice defects with ~ 40 K hysteresis, which has a potential to operate for very large number of transformation cycles.

Slightly more dislocation loops and segments were observed in shape memory tests T5 (Fig. 5a) and T11 (Fig. 8), in which the reverse transformation of oriented martensite took place upon heating at 20 MPa stress.

Compared to the test T8, the wire was deformed in the martensite state to large strain via martensite reorientation, which means that the (001) compound twinned microstructure was rebuilt. For information on the change of the martensitic microstructure upon straining, see [35]. It shall be pointed out that the A_f temperature was shifted 40 °C upwards (Fig. 8b) compared to the thermal cycle (Fig. 6a), and yet practically no lattice defects were created upon cycling in the microstructure and the stress–strain–temperature response was remarkably stable. This upward shift of the A_f temperature (martensite stabilization) is evidently caused by the deformation in martensite taking place without generating unrecovered strain and lattice defects. It is, thus, evident that the martensite stabilization by deformation does not involve any plastic deformation and cannot be ascribed to slip dislocations, as frequently argued in the literature [49]. It is solely due to the additional energy required to form a strain compatible austenite/martensite interfaces on the grain scale within the deformed martensitic microstructure before the reverse transformation takes place on heating [5, 35]. This martensite stabilization by deformation is the reason why the reverse transformation line in the σ-T diagram never coincides with the A_f temperature determined from the DSC or electric resistivity tests on thermally cycled free NiTi wires. Since the forward and reverse martensitic transformations proceed in the absence of stress during the shape memory cycle, very small unrecovered strains, very few permanent lattice defects and no deformation bands were generated upon thermomechanical cycling, in spite of the large stresses and strains applied.

(110)/ < 001 > slip dislocations only were systematically observed in all tests, in which martensitic transformation proceeded at intermediate stresses—T6 (Fig. 5b),
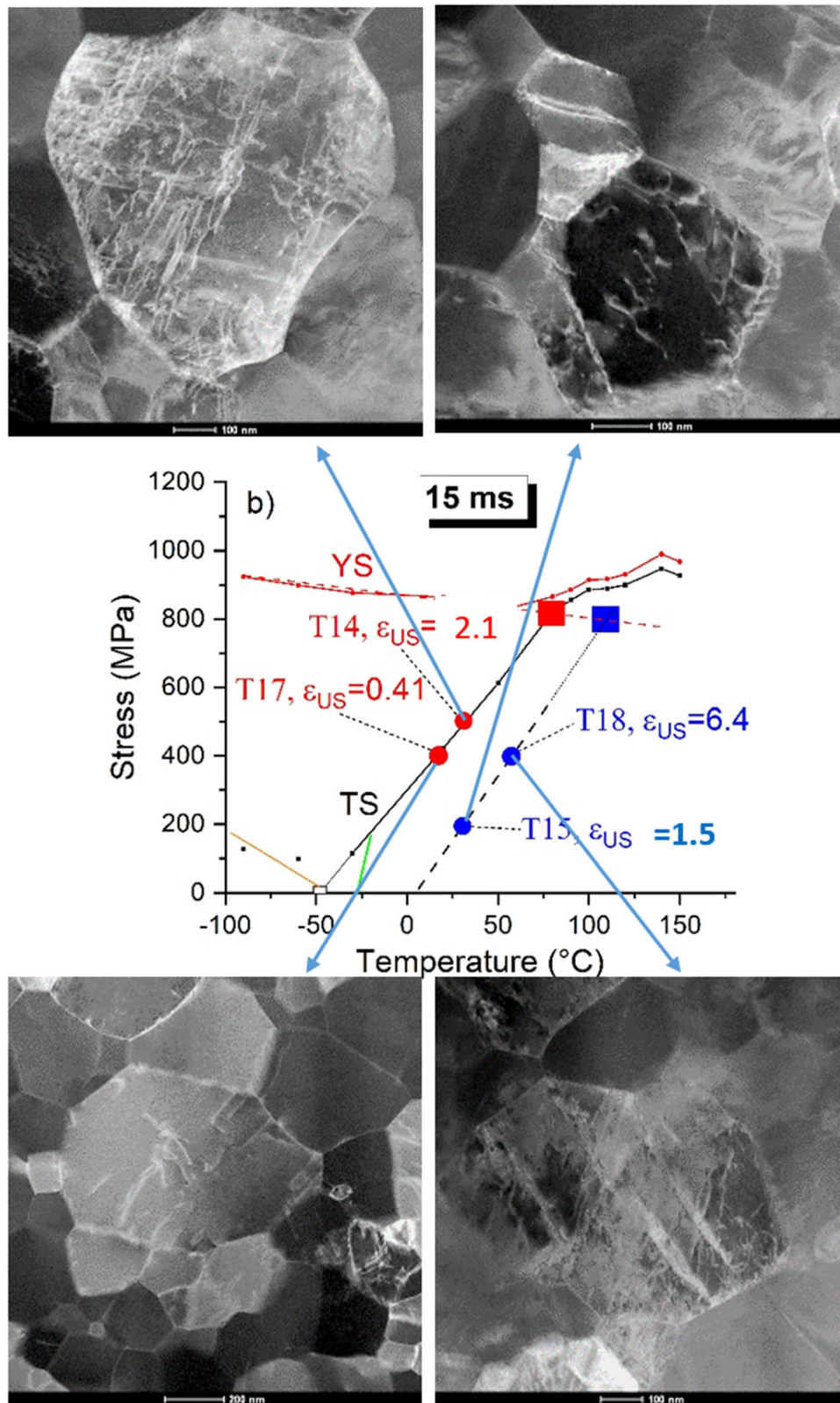
Fig. 14 Unrecovered strain and lattice defects generated in 10 thermomechanical loading bypass cycles in which only forward (T14,T17) or reverse (T15,T18) martensitic transformation proceeds under stress. The unrecovered strains and lattice defects generated during the forward or reverse martensitic transformation are considerably different. While forward transformation on loading is critical (larger unrecovered strain and higher density of dislocation defects) for superelastic cycling, the reverse transformation on heating is critical for thermal cycling under constant stress
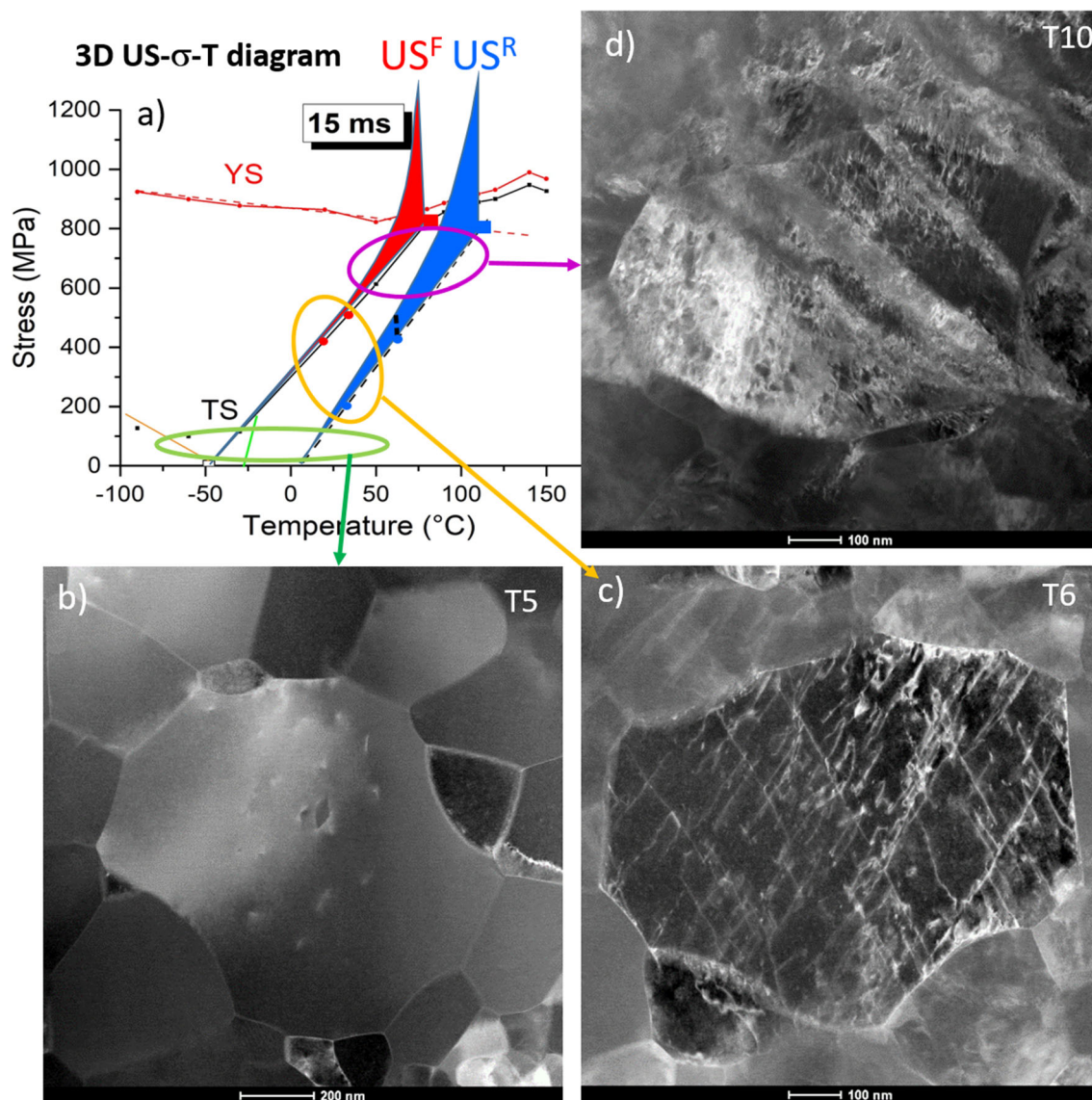
Fig. 15 3D US-σ-T diagram for 15 ms NiTi wire **a** Shows the magnitude of unrecovered strain generated by the forward and reverse martensitic transformations proceeding under denoted stresses/temperatures. Almost no unrecovered strain and very few permanent lattice defects in a form of dislocation loops **b** Were generated in the microstructure when martensitic transformation proceeded at low stresses, **c** Dislocations in {110}/ < 001 > slip system and medium unrecovered strains were generated when martensitic transformation proceeded at intermediate stresses and **d** Deformation bands containing {114} austenite twins and/or single variant residual B19′ martensite plates [7] together with high density of unidentified dislocations were observed when martensitic transformation proceeded at high stresses

T9 (Fig. 6b), T12 (Fig. 9), T13–15 (Fig. 11), T16–18 (Fig. 12). These dislocations were analysed and ascribed to {011}/ < 100 > austenite slip system in our earlier work [13]. Although these slip dislocations were observed to be generated during both forward and reverse transformations in the superelastic cycle (Fig. 11), slightly higher density of slip dislocations was observed during the forward transformation then during the reverse transformation (Fig. 11b, c). Dense dislocation fields were observed - within isolated deformation bands mainly in the tests, in

which the martensitic transformation proceeded at high stresses and temperatures—T7 (Fig. 5c), T10 (Fig. 6c), and T18 (Fig. 12c). These dislocations are different, they probably originate from the dislocation slip on the (001) plane in the B19′ martensite lattice (lattice correspondent plane to the {011} austenite plane) and are inherited by the austenite during the reverse martensitic transformation [35].

There are various theoretical predictions in the literature for the origin of the slip dislocation generated by

superelastic cycling [5, 11, 14, 15, 19, 20]. Several authors claim that the $\{011\}/<100>$ austenite slip dislocations are generated at the propagating habit plane interface at the cross section between the habit planes and type-II twins inside the martensite. Since type-II twins were never observed in stress-induced martensite in nanocrystalline NiTi [35], these predictions cannot explain the observation of the $\{011\}/<100>$ slip dislocations in this work. However, these predictions may still work for NiTi single crystals and solution annealed NiTi. We have proposed earlier [5, 20] that slip dislocations form mainly during the reverse martensitic transformation behind the propagating habit plane interface by the slip in the austenite phase facilitating strain compatibility at the habit plane. This proposition has to be revised as well, since Fig. 11 clearly shows that $011\}/<100>$ slip dislocations are generated during both forward and reverse transformations. An alternative plausible explanation would be that the observed slip dislocations simply form by the activation of the $(110)/<001>$ slip in the austenite matrix due to stress concentrations during the martensitic transformation. Interestingly, the individual $\{110\}/<001>$ dislocations appear mainly in large grains, while isolated single deformation bands are more frequently observed in small grains (Figs. 5b3, 6b3, 9f and 11b3). This most likely originates from different stress states in small and large grains of the transformaing polycrystal. Further theoretical and experimental research is currently in progress to reveal the mechanism by which the slip dislocations actually form during the thermomechanical cycling of nanograined NiTi.

In summary, individual $\{110\}/<001>$ slip dislocations were observed in the microstructure of NiTi wire superelastically or thermally cycled at intermediate stresses, while the recorded accumulated unrecovered strains were relatively low ($\sim$ 2%). The dense dislocation fields, on the other hand, were observed within the isolated deformation bands left in the microstructure of NiTi wire subjected to highest stresses and temperatures in thermomechanical loading tests while the recorded accumulated unrecovered strains were typically very large ($>$ 5%).

Deformation bands were observed mainly in tests, in which martensitic transformation proceeded at high stresses T7 (Fig. 5c), T10 (Fig. 6c), T12 (Fig. 9), T15 (Fig. 11c), T16,18 (Fig. 12a, c). The unrecovered strains recorded in these tests were typically very large ($>$ 2%). The deformation bands contain residual B19$'$ martensite, R-phase or $\{114\}$ austenite twins. The deformation mechanism leading to the creation of deformation bands (and large unrecovered strains) has its origin in the plastic deformation of the oriented B19$'$ martensite phase by (100) deformation twinning [7, 35] and/or kwinking [36] occurring selectively in polycrystal grains experiencing high stresses during the thermomechanical loading tests.

Recent TEM analyses of stress-induced martensite in deformed NiTi reported in the literature [7, 35, 30, 50, 51] suggest that the stress-induced B19$'$ martensite in nanocrystalline NiTi wires is formed by (001) compound twinned single domains of the B19$'$ phase [35]. It is claimed in [35] that the dislocation slip on the (001) plane in the B19$'$ martensite lattice is likely to occur at elevated stresses. Sittner et al. [7] identified the interfaces separating the B19$'$ deformation bands from the B2 austenite matrix in the residual martensite observed in a very similar 16 ms NiTi wire subjected to two superelastic cycles as the $(-21-1)$B2//(10-1)B19$'$ interfaces. Two martensite variants forming the (20-1)B19$'$ deformation twin in Fig. 2 in Ref. [30] are separated from the surrounding austenite matrix by the same interface. Casalena et al. [50] recently observed this interface in the microstructure of NiTiHf alloy subjected to 10 superelastic cycles at room temperature. Although these interfaces are not strain compatible and shall not exist in NiTi from theoretical point of view [1], they were regularly observed experimentally in deformed NiTi alloys. We suspect that (100) deformation twinning in overstressed B19$'$ martensite is responsible for initiation of residual martensite bands [7, 35] upon cyclic superelastic loading (Fig. 11) and actuator cycling (Fig. 12).

The microstructure observed in some tests (Fig. 6c), however, contains a very large density of deformation bands and very large unrecovered strains introduced by the kwinking deformation [36] mentioned in the introduction. The kwinking (combination of deformation twinning and dislocation-based kinking in the B19$'$ martensite) was claimed to be responsible for the onset of plastic yielding of martensite [35] (Fig. 1a). It gives rise to the deformation bands containing $\{114\}$ austenite twins in the microstructure of the wire observed by TEM after unloading and heating above A_f temperature [7, 34]. We originally treated the deformation mechanism leading to the creation of deformation bands as deformation twinning in the B19$'$ martensite followed by reverse transformation of the crystal within the band to the austenite twin [7, 34]. But there is high density of slip dislocations within the deformation bands (e.g. Figs. 11a4 and Fig. 12a4) as well as in the surrounding austenite matrix (Fig. 6c), which needs to be taken into account. Later on, we have realized that this localized deformation involves combination of deformation twinning and dislocation-based kinking, called kwinking in [36]. Since the kwinking deformation takes place, when the material is loaded in the martensite phase, it can take place during the forward and/or reverse transformation, whenever the stress acting on the B19$'$ martensite locally increases in thermomechanical loading tests.

As introduced in [36], kwinking deformation leads to mesoscopically localized plastic deformation of the stress-

induced martensite. It may occur during the forward loading (or cooling under large stress), during loading in martensite state or during the reverse transformation upon reverse unloading (or heating under large stress). In fact, the results of the bypass experiments seem to suggest that deformation bands tend to appear preferentially during the reverse transformation on unloading and heating (Fig. 14). Hence, unrecovered strain and deformation bands accumulate upon thermomechanical cycling involving heating under large stress (Fig. 12c). In case of reverse martensitic transformation proceeding under very large temperature/stress (Fig. 6c), the wire almost did not shorten upon heating under 750 MPa stress. The detailed mechanism of the kwinking deformation accompanying the cyclic martensitic transformation yet remains to be investigated both experimentally and theoretically. It was observed that the martensite lattice within the deformation band transforms to the {114} austenite twins upon the constrained heating to high temperatures [7, 20, 35]. The austenite phase is, thus, completely restored during the reverse transformation upon heating but large unrecovered strain remains. Reverse martensitic transformation upon heating proceeding into austenite twins within the deformation bands [7, 20, 32, 41] is considered to play key role in this.

In summary, the deformation bands observed in the microstructure of NiTi wire subjected to thermomechanical cycling at high temperatures/stresses correlate with very large unrecovered strains recorded in these tests. The deformation mechanism by which the deformation bands are created is related to the (100) deformation twinning [7, 35] and/or kwinking deformation [35, 36] in oriented B19′ martensite.

The Effect of Temperature/Stress at Which the Forward and Reverse Martensitic Transformations Take Place

The results of tests T5–T7 (Fig. 5) and T8–T10 (Fig. 6) provide clear evidence that the amount of unrecovered strains and permanent lattice defects recorded after 10 closed-loop cycles dramatically increases with increasing temperature and stress, at which the martensitic transformation proceeds. As concerns unrecovered strains, we knew that already from the previous work [5]. New information brought in by the present experiments is that the type and density of lattice defects vary with the increasing temperature and stress as well.

The conventional superelastic and thermal cycles, in which martensitic transformation proceeded at medium stresses (Fig. 13), show that the observed unrecovered strains and lattice defects are comparable in superelastic cycling and thermal cycling if they take place at comparable temperatures/stresses. The problem is that, the

forward and reverse transformations proceed at different temperatures/stresses (Fig. 13) and analysis of unrecovered strains and lattice defects from the conventional tests T5–T10 is impossible. We knew from the results of [5] that the amount of unrecovered strain generated in a single thermomechanical loading cycle on NiTi wire can be evaluated separately for the forward and reverse transformations by employing bypass tests. A problem is that the first cycle cannot be taken as representative for defect generation upon cycling. Deformation bands frequently appear in 2nd, 5th, 10th (and possibly 1000th) cycle. The bypass test analysis was applied to cyclic loading tests T13–T15 (Figs. 10a and 11) and T14–T18 (Figs. 10b and 12) to determine unrecovered strains and permanent lattice defects created by the cyclic forward and reverse transformations, separately (Figs. 10, 11, 12, 13, 14 and 15).

Let us discuss the results of the cyclic bypass tests with the help of Figs. 14 and 15, in which the unrecovered strains and lattice defects generated by martensitic transformation proceeding at denoted [temperature, stress] conditions are presented. The 3D US-σ-T diagram in Fig. 15 shows unrecovered strains accumulated in 10 thermomechanical loading bypass cycles, in which forward or reverse martensitic transformation proceeded at [temperature, stress] conditions denoted by transformation lines in stress–temperature space. The diagram is just a sketch (adopted from [5]) reflecting the experimental data in Fig. 14.

The upper plateau transformation stress is generally considered in the SMA field to be relevant for estimating functional fatigue of NiTi wires. In this respect, it is somehow surprising to learn that roughly equal unrecovered strains (and permanent lattice defects) were generated during the forward and reverse martensitic transformations in the superelastic cycling, even if the forward transformation stress is much higher than the reverse one. At the same time, much larger unrecovered strains were generated during the reverse martensitic transformation in the actuation cycle, in which both forward and reverse transformations proceed at equal stresses. This is reflected by the shape of the US curves in the 3D US-σ-T diagram (Fig. 15),

There is large difference between lattice defects generated by the forward and reverse martensitic transformations in the thermal cycling at constant stress 400 MPa (Fig. 12). The unrecovered strain generated during 10 cycles through forward transformation under stress (T17) was only 0.41%, while that generated through the reverse transformation (T18) was 6.4%. The permanent lattice defects observed in T17 and T18 are very different as well. The plastic deformation upon thermal cycling under stress, thus, takes place mainly during the heating and the strain–temperature response upon heating, thus, gradually shifts towards lower

temperatures during the 10 cycles (T16 in Fig. 12a). However, it also probably depends on the applied stress, since the strain–temperature response upon thermal cycling under 280 MPa (T9 in Fig. 6b) shifts on both cooling and heating sides, suggesting similar lattice defects and unrecovered strains generated during the forward and reverse transformations. In this case, however, no deformation bands were found in the microstructure of the cycled wire (Fig. 6b). Obviously, these results are of key importance for the design of NiTi actuators.

It is interesting to see that gradual evolution of stress–strain–temperature response upon cycling (cyclic instability) reflects the accumulation of unrecovered strains and lattice defects by the forward and/or reverse martensitic transformations. In case of the cyclic superelastic stress–strain curves, this frequently means that the hysteresis decreases because the forward transformation stress decreases upon cycling (see Figs. 1c, d and 5b). In case of the strain–temperature response upon thermal cycling under stress, this frequently means that the hysteresis width decreases because of the shift of the strain recovery upon heating to lower temperatures (see Fig. 12a). Nevertheless, it shall be pointed out that superelastic cycling at constant temperature and thermal cycling under constant stress are special cases of general cyclic thermomechanical loading tests, which include also cyclic shape memory tests, recovery stress tests. The 3D US-σ-T diagram represents a unique tool enabling to estimate cyclic instability of NiTi in any general thermomechanical loading test.

The three colour ellipses drawn in the 3D US-σ-T diagram in Fig. 15 denote [temperature, stress] conditions under which very different unrecovered strains and lattice defects were observed (tests T5,T6,T10). The observed lattice defects are discussed in Sect. "Permanent lattice defects". Since the deformation bands were created by cyclic plastic deformation processes in the martensite phase, analysis of martensitic microstructures in cyclically deformed wires would be necessary to reveal their origin in detail. The reader can find relevant information on the martensitic microstructures in thermomechanical tests on a similar NiTi wire in [35], but further research is required to reveal the mechanism by which the deformation bands are created by cyclic martensitic transformation under elevated stresses.

Based on the 3D US-σ-T diagram, we can understand why cyclically stable superelasticity is in fact hardly achievable for the 15 ms NiTi wire, but it is relatively easy to achieve stable cyclic strain–temperature responses in thermal cycling under constant stress. In other words, we can understand why commercial NiTi wires can survive millions of thermal cycles under constant stress but only thousands of superelastic cycles. To achieve cyclic stability in thermomechanical loading tests on NiTi wires, the temperatures/

stresses at which martensitic transformation proceeds have to be kept under some critical values to prevent generation of unrecovered strains and permanent lattice defects. It shall be pointed out that the 15 ms NiTi is a model alloy, on which the permanent lattice defects could be beneficially investigated. The commercial superelastic NiTi wires are much stronger (YS > 1300 MPa) and the values of the critical stresses/temperatures are hence higher [5, 37].

The Effect of Virgin Austenitic Microstructure

It is well known that functional responses of NiTi wires depend on the virgin austenitic microstructure [37]. Although the present experiments were performed only on the 15 ms NiTi wire with optimized microstructure, we would like to discuss briefly the effect of the virgin austenitic microstructure on the stability of cyclic functional behaviour of NiTi wires because this is after all of the main importance for engineering applications of NiTi wires.

We use the term "microstructure" in a general sense covering grain size, dislocations, twins, precipitates, internal stress and texture of the wire. In the SMA modelling literature, however, the meaning of the term microstructure is frequently reduced to the grain size. In reality, however, excluding NiTi wires with partially recrystallized microstructures having grain size below 100 nm [52, 53], the superelastic stress–strain response of NiTi is only slightly affected by the grain size, but the cyclic instability of the stress–strain response varies dramatically with the grain size, since the yield stress for plastic deformation of martensite decreases with increasing grain size [13, 37].

In view of the anticipated impact of the yield stress for plastic deformation of martensite on the cyclic stability, we have introduced the material parameter YS determined as the yield stress σ^Y needed to trigger the plastic deformation of martensite in tensile test (Fig. 1a). While the parameter YS decreases only slightly with the increasing test temperature, the transformation stress TS increases with increasing temperature with ~ 6 MPa/°C rate as common for NiTi (Fig. 2c). Since generation of unrecovered strains and lattice defects is different during the forward and reverse martensitic transformations (Figs. 14 and 15), we propose to use a parameter

$$YT^{F,R} = ||[\sigma^*, T^*] - [\sigma, T]^{F,R}|| \qquad (1)$$

$YT^{F,R}$ are actually the distances from the $[\sigma,T]^{F,R}$ states (at which the transformation proceeds) to the critical states $[\sigma^*,T^*]^{F,R}$ (at which the forward (reverse) transformation line meets the Yield stress line in the σ-T diagram). The shorter the distance is, the larger is the unrecovered strain (Fig. 14 and 15) and the more unstable will be the cyclic stress–strain–temperature response of the NiTi wire in the

thermomechanical loading test passing through the $[\sigma,T]^{F,R}$ states. Based on the parameters $YT^{F,R}$ for given thermomechanical loading test and 3D US-σ-T diagram, one can estimate the cyclic instability of any NiTi wire in any thermomechanical loading test.

This scheme makes it possible to fully understand the results of our earlier work [13] focussed on the TEM analysis of lattice defects in NiTi wires with range of microstructures subjected to 10 superelastic cycles at room temperature. While no evidence for dislocation slip was observed in 12 ms NiTi wires with small grain size '∼50 nm, pronounced activity of dislocation slip in three austenite slip systems {0 1 1}/< 100 > was observed in 16 ms NiTi wires with ∼ 500 nm mean grain size, the {114} austenite twins were observed only in 18 ms NiTi wires with the largest mean grain size ∼ 1000 nm. The 3D US-σ-T diagram of these three wires would be very different.

The key advantage of this scheme is thus that it can be used to estimate the cyclic instability of stress–strain–temperature response of various NiTi alloys (various compositions given various cold works/heat treatments) subjected to any kind of cyclic thermomechanical loading tests. Transformation stress TS at given temperature for a particular wire depends mainly on the chemical composition of the alloy. The yield stress YS (varies between ∼ 2000 MPa and ∼ 500 MPa with the heat treatment [37]) depends significantly on the grain size. This is because the plastic yielding is due to combined deformation twinning and dislocation-based kinking [35] constituting the kwinking deformation mechanism [36], which is very sensitive to the grain size. In case of NiTi wires with small grain size, massive activity of this deformation mechanism leads to strain localization, necking and fracture at ∼ 13–15% strain [37]. The cyclic instability of any NiTi wire in any thermomechanical loading test, thus, depends on the type of the wire (characterized by YS, TS) and type of the applied test (characterized by TS).

There are three basic approaches to achieve cyclically more stable stress–strain–temperature response from NiTi shape memory alloy. First, classical one consists in strengthening the wire to push the yield stress YS up as much as possible, second is to determine the 3D US-σ-T diagram and perform the thermomechanical loading in such a way that the martensitic transformation takes place under conditions, at which no unrecovered strains and lattice defects are generated. Third approach would require to discover the mechanisms by which the slip dislocations are generated by the martensitic transformation and try to modify the martensitic transformation (modify lattice parameters of involved phases by adjusting chemical composition) so that it does not generate unrecovered strain and permanent lattice defects when it proceeds cyclically

under large stress [54–56]. All three approaches can be beneficially combined.

Conclusions

Series of cyclic thermomechanical loading tests (10 closed-loop cycles) on superelastic NiTi wire with recrystallized nanograined microstructure (15 ms NiTi wire) was performed to investigate the origin of the cyclic instability of functional behaviours of NiTi.

The cyclic stress–strain–temperature responses of the wire were found:

- relatively stable, generating only marginal accumulated unrecovered strain and/or few isolated lattice defects, if the both the forward and reverse martensitic transformations proceed at low stress (<100 MPa)
- very unstable, generating significant accumulated unrecovered strain and high density of slip dislocations and deformation bands, if the forward and/or reverse martensitic transformation proceeded under large external stress (>250 MPa).

The recorded accumulated unrecovered strains and density of permanent lattice defects increased with increasing temperature/stress, at which the forward and/or reverse martensitic transformation proceeded in the test. It did not correlate with the temperature and stress applied in the test as such.

The type of permanent lattice defects observed in the microstructure of the cycled wire by TEM was found to depend on the temperature/stress, at which the forward and reverse martensitic transformations proceeded in the test, in particular:

- at low stresses (<100 MPa), the cyclic martensitic transformation generated only few dislocation loops and segments and the recorded accumulated unrecovered strains were negligible (< 0.1%)
- at intermediate stresses (100 MPa < σ < 400 MPa), high density of (110)/< 001 > slip dislocations and few isolated deformation bands were observed in the microstructure and accumulated unrecovered strains reached few per cent (∼ 0.5–2%)
- at high stresses (400 MPa < σ), deformation bands containing B19′ martensite and/or {114} austenite twins alongside high density of slip dislocations were observed in the microstructure and accumulated unrecovered strains became very large (> > 2%)

3D US-σ-T diagram providing information on unrecovered strain generated by the martensitic transformation proceeding at given temperature and stress constructed from the results of the bypass tests enables prediction of the

cyclic instability of stress–strain–temperature functional behaviour of various NiTi wire subjected to general thermomechanical loading tests.

References

1. Otsuka K, Ren X (2005) Physical metallurgy of Ti–Ni-based shape memory alloys. Prog Mater Sci 50:511–678. https://doi.org/10.1016/j.pmatsci.2004.10.001

2. Melton KN (1990) Ni-Ti based shape memory alloys. In: Duerig TW, Melton KN, Stoeckel D, Wayman CM (eds) Engineering aspects of shape memory alloys. Butterworth-Heinmann, England, pp 21–35

3. Miyazaki S (1990) Thermal and stress cycling effects and fatigue properties of Ni-Ti alloys. In: Duerig TW, Melton KN, Stoeckel D, Wayman CM (eds) Engineering aspects of shape memory alloys. Butterworth-Heinmann, England, pp 394–413

4. Sedmak P, Šittner P, Pilch J, Curfs C (2015) Instability of cyclic superelastic deformation of NiTi investigated by synchrotron X-ray diffraction. Acta Materialia 94:257–270. https://doi.org/10.1016/J.ACTAMAT.2015.04.039

5. Heller L, Seiner H, Šittner P, Sedlák P, Tyc O, Kadeřávek L (2018) On the plastic deformation accompanying cyclic martensitic transformation in thermomechanically loaded NiTi. Int J Plast 111:53–71. https://doi.org/10.1016/j.ijplas.2018.07.007

6. Chen Y, Tyc O, Kadeřávek L, Molnárová O, Heller L, Šittner P (2019) Temperature and microstructure dependence of localized tensile deformation of superelastic NiTi wires. Mater Des 174:107797. https://doi.org/10.1016/j.matdes.2019.107797

7. Šittner P, Molnárová O, Kadeřávek L, Tyc O, Heller L (2020) Deformation twinning in martensite affecting functional behaviour of NiTi shape memory alloys. Materialia 9:100506. https://doi.org/10.1016/j.mtla.2019.100506

8. Eggeler G, Hornbogen E, Yawny A, Heckmann A, Wagner M (2004) Structural and functional fatigue of NiTi shape memory alloys. Mater Sci Eng A 378:24–33. https://doi.org/10.1016/J.MSEA.2003.10.327

9. Robertson SW, Pelton AR, Ritchie RO (2012) Mechanical fatigue and fracture of Nitinol. Int Mater Rev 57:1–36. https://doi.org/10.1179/1743280411Y.0000000009

10. Frenzel J (2020) On the importance of structural and functional fatigue in shape memory technology. Shap Mem Superelasticity 6:213–222. https://doi.org/10.1007/s40830-020-00281-3

11. Simon T, Kroger A, Somsen C, Dlouhy A, Eggeler G (2010) On the multiplication of dislocations during martensitic transformations in NiTi shape memory alloys. Acta Mater 58:1850–1860

12. Hurley J, Ortega AM, Lechniak J, Gall K, Maier HJ (2003) Structural evolution during the cycling of NiTi shape memory alloys. Int J Mater Res 94:547–552. https://doi.org/10.3139/146.030547

13. Delville R, Malard B, Pilch J, Sittner P, Schryvers D (2011) Transmission electron microscopy investigation of dislocation slip during superelastic cycling of Ni–Ti wires. Int J Plast 27:282–297. https://doi.org/10.1016/J.IJPLAS.2010.05.005

14. Norfleet DM, Sarosi PM, Manchiraju S, Wagner MFX, Uchic MD, Anderson PM, Mills MJ (2009) Transformation-induced plasticity during pseudoelasticdeformation in Ni-Ti microcrystals. Acta Mater 57:3549–3561. https://doi.org/10.1016/j.actamat.2009.04.009

15. Bowers ML, Chen X, De Graef M, Anderson PM, Mills MJ (2014) Characterization and modeling of defects generated in pseudoelastically deformed NiTi microcrystals. Scr Mater. https://doi.org/10.1016/j.scriptamat.2014.02.001

16. Ezaz T, Wang J, Sehitoglu H, Maier HJ (2013) Plastic deformation of NiTi shape memory alloys. Acta Mater 61:67–78. https://doi.org/10.1016/j.actamat.2012.09.023

17. Polatidis E, Šmíd M, Kuběna I, Hsu WN, Laplanche G, Van Swygenhoven H (2020) Deformation mechanisms in a superelastic NiTi alloy: An in-situ high resolution digital image correlation study. Mater Design 191:108622. https://doi.org/10.1016/j.matdes.2020.108622

18. Chowdhury P, Sehitoglu H (2017) Deformation physics of shape memory alloys—Fundamentals at atomistic frontier. Prog Mater Sci 88:49–88. https://doi.org/10.1016/J.PMATSCI.2017.03.003

19. Paranjape HM, Bowers ML, Mills MJ, Anderson PM (2017) Mechanisms for phase transformation induced slip in shape memory alloy micro-crystals. Acta Mater 132:444–454. https://doi.org/10.1016/j.actamat.2017.04.066

20. Šittner P, Sedlák P, Seiner H, Sedmák P, Pilch J, Delville R, Heller L, Kadeřávek L (2018) On the coupling between martensitic transformation and plasticity in NiTi: experiments and continuum based modelling. Prog Mater Sci 98:249–298. https://doi.org/10.1016/j.pmatsci.2018.07.003

21. Šittner P, Heller L, Sedlák P, Chen Y, Tyc O, Molnárová O, Kadeřávek L (2019) B2 $\Rightarrow$ B19$'$ $\Rightarrow$ B2T martensitic transformation as a mechanism of plastic deformation of NiTi. Shap Mem Superelasticity 5:383–396. https://doi.org/10.1007/s40830-019-00250-5

22. Hsu WN, Polatidis E, Smíd M, Van Petegem S, Casati N, Van Swygenhoven H (2019) Deformation and degradation of superelastic NiTi under multiaxialloading. Acta Mater 167:149–158

23. Bian X, Saleh AA, Pereloma EV, Davies CHJ, Gazder AA (2018) A digital image correlation study of a NiTi alloy subjected to monotonic uniaxial and cyclic loading-unloading in tension. Mater Sci Eng A. https://doi.org/10.1016/j.msea.2018.04.081

24. Sehitoglu H, Wu Y, Alkan S, Ertekin E (2017) Plastic deformation of B2-NiTi—is it slip or twinning? Phil Mag Lett 97:217–228. https://doi.org/10.1080/09500839.2017.1316019

25. Chowdhury P, Sehitoglu H (2017) Revisit to atomistic rationale for slip in shape memory alloys. Prog Mater Sci 85:1–42

26. Goo E, Duerig T, Melton K, Sinclair R (1985) Mechanical twinning in Ti50Ni47Fe3 and Ti49Ni51 alloys. Acta Metall 33:1725–1733. https://doi.org/10.1016/0001-6160(85)90167-1

27. Tyumentsev AN, Surikova NS, Litovchenko IY, Pinzhin YP, Korotaev AD, Lysenko OV (2004) Mechanism of deformation and crystal lattice reorientation in strain localization bands and deformation twins of the B2 phase of titanium nickelide. Acta Mater 52:2067–2074. https://doi.org/10.1016/J.ACTAMAT.2004.01.001

28. Karaman I, Karaman I, Kulkarni AV, Luo ZP (2005) Transformation behaviour and unusual twinning in a NiTi shape memory alloy ausformed using equal channel angular extrusion. Philos Mag 85:1729–1745. https://doi.org/10.1080/14786430412331331961

29. Nishida M, Matsuda M, Fujimoto T, Tanaka K, Kakisaka A, Nakashima H (2006) Crystallography of deformation twin boundaries in a B2 type Ti–Ni alloy. Mater Sci Eng, A 438–440:495–499. https://doi.org/10.1016/j.msea.2006.03.111

30. Ii S, Yamauchi K, Maruhashi Y, Nishida M (2003) Direct evidence of correlation between {2 0 $\bar{1}$}B19′ and {1 1 4}B2 deformation twins in Ti–Ni shape memory alloy. Scr Mater 49:723–727. https://doi.org/10.1016/S1359-6462(03)00356-7

31. Moberly WJ, Proft JL, Duerig TW, Sinclair R (1990) Deformation, twinning and thermo-mechanical strengthening of Ti50Ni47Fe3. Acta Metall Mater 38:2601–2612. https://doi.org/10.1016/0956-7151(90)90272-I

32. Gao Y (2019) Symmetry and pathway analyses of the twinning 1 modes in Ni-Ti shape memory alloys. Materialia 6:100320. https://doi.org/10.1016/j.mtla.2019.100320

33. Zhang JX, Sato M, Ishida A (2006) Deformation mechanism of martensite in Ti-rich Ti–Ni shape memory alloy thin films. Acta Mater 54:1185–1198. https://doi.org/10.1016/j.actamat.2005.10.046

34. Chen Y, Tyc O, Kadeřávek L, Molnárová O, Heller L, Šittner P (2019) Recoverability of large strains and deformation twinning in martensite during tensile deformation of NiTi shape memory alloy polycrystals. Acta Mater 180:243–259. https://doi.org/10.1016/j.actamat.2019.09.012

35. Molnárová O, Tyc O, Heller L, Seiner H, Šittner P (2021) 3D Reconstruction of martensitic microstructures in grains of deformed nanocrystalline NiTi wires by TEM. Acta Mater (submitted). Available at SSRN: https://ssrn.com/abstract=3797420

36. H Seiner, P Sedlák, L Heller, O Molnárová, P Šittner. On the origin of (20–1) interfaces in B19' NiTi martensite, in preparation, H. Seiner, The (2$\bar{0}$1) interfaces in plastically formed NiTi martensite - twins or 'kwinks'? Presentation available online from ASM international, www.asminternational.org/news/videos/-/journal_content/56/10192/42847968/VIDEO

37. Chen Y, Tyc O, Molnárová O, Heller L, Šittner P (2019) Tensile deformation of superelastic NiTi wires in wide temperature and microstructure ranges. Shap Mem Superelasticity 5:42–62. https://doi.org/10.1007/s40830-018-00205-2

38. Sedmák P, Pilch J, Heller L, Kopeček J, Wright J, Sedlák P et al (2016) Grain-resolved analysis of localized deformation in nickel-titanium wire under tensile load. Science 353:559–562. https://doi.org/10.1126/science.aad6700

39. Tyc O, Heller L, Vronka M, Sittner P (2020) Effect of temperature on fatigue of superelastic NiTi wires. Int J Fatigue 134:105470. https://doi.org/10.1016/j.ijfatigue.2020.105470

40. Pourbabak S, Verlinden B, Van Humbeeck J, Schryvers D (2020) DSC cycling effects on phase transformation temperatures of micron and submicron grain Ni50.8Ti49.2 microwires. Shap Mem Superelasticity 6:232–241. https://doi.org/10.1007/s40830-020-00278-y

41. Heller L, Šittner P, Sedlák P, Seiner H, Tyc O, Kadeřávek L, Sedmák P, Vronka M (2019) Beyond the strain recoverability of martensitic transformation in NiTi. Int J Plast 116:232–264. https://doi.org/10.1016/j.ijplas.2019.01.007

42. Zhao TX, Kang GZ, Yu CH, Kan QH (2019) Experimental investigation of the cyclic degradation of the one-way shape memory effect of NiTi alloys. Int J Miner Metall Mat 26:1539. https://doi.org/10.1007/s12613-019-1884-8

43. Šittner P, Vokoun D, Dayananda GN, Stalmans R (2000) Recovery stress generation in shape memory Ti50Ni45Cu5 thin wires. Mater Sci Eng, A 286:298–311. https://doi.org/10.1016/S0921-5093(00)00816-9

44. Liu Y, Xie Z (2007) Detwinning in shape memory alloy. In: Progress in smart materials and structures. Nova Science Publishers, Inc

45. Liu Y, Xie Z (2003) Twinning and detwinning of 0 1 1type II twin in shape memory alloy. Acta Mater 51:5529–5543

46. Waitz T (2005) The self-accommodated morphology of martensite in nanocrystalline NiTi shape memory alloys. Acta Mater 53:2273–2283. https://doi.org/10.1016/j.actamat.2005.01.033

47. Petersmann M, Antretter T, Waitz T (2015) Special cases of martensite compatibility: a near single-variant habitplane and the martensite of nanocrystalline NiTi. MATEC Web Conf 33:03015. https://doi.org/10.1051/matecconf/20153303015

48. Waitz T, Antretter T, Fischer FD, Karnthaler HP (2008) Size effects on martensitic phase transformations in nanocrystalline NiTi shape memory alloys. Mat Sci Technol. https://doi.org/10.1179/174328408X302620

49. Liu Y, Tan G, Miyazaki S (2006) Deformation-induced martensite stabilisation in [1 0 0] single-crystalline Ni–Ti. Mater Sci Eng A438–440:612–616. https://doi.org/10.1016/j.msea.2006.02.130

50. Casalena L, Bucsek AN, Pagan DC, Hommer GM, Bigelow GS, Obstalecki M, Noebe RD, Mills MJ, Stebner AP (2018) Structure-property relationships of a high strength superelastic NiTi–1Hf alloy. Adv Eng Mater 20:1800046. https://doi.org/10.1002/adem.201800046

51. Tirry W, Schryvers D (2008) In situ transmission electron microscopy of stress-induced martensite with focus on martensite twinning. Mater Sci Eng A 481–482:420–425. https://doi.org/10.1016/j.msea.2006.12.214

52. Ahadi A, Sun Q (2014) Effects of grain size on the rate-dependent thermomechanical responses of nanostructured superelastic NiTi. Acta Materialia 76:186–197. https://doi.org/10.1016/j.actamat.2014.05.007

53. Chen J, Wu Y, Yin H (2020) In situ multi-field investigation of grain size effects on the rate dependent thermomechanical responses of polycrystalline superelastic NiTi. Mater Lett 259:126845. https://doi.org/10.1016/j.matlet.2019.126845

54. James RD (2015) Taming the temperamental metal transformation. Science 348:968–969. https://doi.org/10.1126/science.aab3273

55. Chluba C, Ge W, Lima de Miranda R, Strobel J, Kienle L, Quandt E, Wuttig M (2015) Ultralow-fatigue shape memory alloy films. Science 348:1004. https://doi.org/10.1126/science.1261164

56. Bumke L, Zamponi CH, Jetter J, Quandt E (2020) Cu-rich Ti52.8Ni22.2Cu22.5Co2.5 shape memory alloy films with ultra-low fatigue for elastocaloric applications reference citations were renumbered including their corresponding references in the reference list. Please check if action taken is appropriate. Otherwise, kindly advise us on how to proceed. J Appl Phys 127:225105. https://doi.org/10.1063/5.0006301